Hierarchical activation of compartmentalized pools of AMPK depends on severity of nutrient or energy stress

Zong, Yue; Zhang, Chen-Song; Li, Mengqi; Wang, Wen; Wang, Zhichao; Hawley, Simon A.

Published in:
Cell Research

DOI:
10.1038/s41422-019-0163-6

Publication date:
2019

Document Version
Peer reviewed version

Hierarchical activation of compartmentalized pools of AMPK depends on severity of nutrient or energy stress

Yue Zong[1], Chen-Song Zhang[1], Mengqi Li[1], Wen Wang[2,3], Zhichao Wang[2,3], Simon A. Hawley[4], Teng Ma[1], Jin-Wei Feng[1], Xiao Tian[1], Qu Qi[1], Yu-Qing Wu[1], Cixiong Zhang[1], Zhiyun Ye[1], Shu-Yong Lin[1], Hai-Long Piao[2,3], D. Grahame Hardie[4], and Sheng-Cai Lin[1]

[1]State Key Laboratory for Cellular Stress Biology, School of Life Sciences, Xiamen University, Fujian 361102, China

[2]Scientific Research Center for Translational Medicine, Dalian Institute of Chemical Physics, Chinese Academy of Sciences, Dalian 116023, China

[3]University of Chinese Academy of Sciences, Beijing 100049, China

[4]Division of Cell Signalling and Immunology, College of Life Sciences, University of Dundee, Dundee DD1 5EH, Scotland, UK

Correspondence: Sheng-Cai Lin (linsc@xmu.edu.cn)

These authors contributed equally: Yue Zong, Chen-Song Zhang Mengqi Li, Wen Wang

AMPK, a master regulator of metabolic homeostasis, is activated by both AMP-dependent and AMP-independent mechanisms. We investigated the conditions under which these different mechanisms operate, and their biological

implications. We show that, depending on the degree of elevation of cellular AMP, distinct compartmentalized pools of AMPK are activated, phosphorylating different sets of targets. Low glucose activates AMPK exclusively through the AMP-independent, AXIN-based pathway in lysosomes to phosphorylate targets such as ACC1 and SREBP1c, exerting early anti-anabolic and pro-catabolic roles. Moderate increases in AMP expand this to activation of cytosolic AMPK although still AXIN-dependent, while high concentrations of AMP arising from severe nutrient stress activates all pools of AMPK independently of AXIN. Surprisingly, mitochondrion-localized AMPK is activated, and phosphorylates ACC2 and mitochondrial fission factor (MFF), only during severe nutrient stress. Our findings reveal a spatiotemporal basis for hierarchical activation of different pools of AMPK during differing degrees of severity of stress.

INTRODUCTION

The AMP-activated protein kinase (AMPK) is a pivotal sensor for monitoring cellular nutrient supply and energy status, and plays crucial roles in adaptive responses to nutrient availability and falling energy levels[1-5]. AMPK occurs as heterotrimeric complexes containing a catalytic α subunit and regulatory β and γ subunits, with the γ subunit providing the binding sites for the regulatory adenine nucleotides AMP, ADP and ATP, their occupancy depending on the cellular AMP:ATP and ADP:ATP ratios[6-8]. Binding of AMP causes allosteric activation of AMPK, while binding of AMP or ADP enhances phosphorylation of Thr172 on the α subunit by the upstream

kinase liver kinase B1 (LKB1), and inhibits Thr172 dephosphorylation by protein phosphatases; all three effects being opposed by binding of ATP[9]. This represents the classical or canonical mechanism for activation. Thr172 can also be phosphorylated by a non-canonical, AMP/ADP-independent mechanism in which Thr172 is phosphorylated by the alternative upstream kinase Ca^{2+}/calmodulin-dependent protein kinase kinase-2 (CaMKK2/CaMKKβ) in response to increases in cellular Ca^{2+} concentration[10-12]. Glucose starvation of cells has been known for many years to activate AMPK[13], and was believed to occur exclusively via the canonical mechanism involving increases in cellular AMP or ADP. However, this view has been challenged by recent findings that AMPK located at the lysosome can be activated by falling levels of glucose, both in vivo and in vitro, via an additional AMP/ADP-independent mechanism[14, 15]. This mechanism requires the glycolytic enzyme fructose-1,6-bisphosphate (FBP) aldolase, the vacuolar H^+-ATPase (v-ATPase), the pentameric Ragulator complex (LAMTOR1-LAMTOR5[16, 17]), and the scaffold protein AXIN1 (often referred to simply as AXIN), which binds the upstream kinase LKB1. As glucose in the medium is reduced, aldolase associated with the v-ATPase becomes progressively unoccupied by FBP, and this transmits the signal of glucose shortage to the v-ATPase:Ragulator complex. The latter then undergoes conformational changes that allow binding of the AXIN1-LKB1 complex, which in turn forms a complex with AMPK at the lysosome. This “super-complex”, referred to below as the lysosomal AMPK activation complex, brings LKB1 and AMPK together, leading to phosphorylation and activation of the latter[4, 14, 18, 19]. Besides AMPK

67 located at the lysosome, subcellular fractionation and fluorescence microscopy
68 analyses have shown that AMPK can be localized and activated in other locations
69 such as the cytosol, nucleus and mitochondria, both in mammalian cells and in
70 yeast[20-26]. Importantly, N-myristoylation of AMPK-β subunits[27, 28] has been shown to
71 be necessary for lysosomal localization and activation of AMPK in an
72 AMP-independent manner by glucose starvation[14], as well as for mitochondrial
73 localization and induction of mitophagy in various mammalian cell lines[24].
74
75 Once activated, AMPK directly phosphorylates multiple targets involved in regulation
76 of metabolic processes to maintain energy homeostasis. These effects can be
77 categorized as: i) inhibition of anabolism, and ii) stimulation of catabolism, thus
78 minimizing ATP consumption and stimulating ATP production respectively[3]. For
79 example, AMPK phosphorylates and inactivates both isoforms of acetyl-CoA
80 carboxylase, i.e. ACC1 (on Ser79[29]) and ACC2 (on Ser221[30]). These isoforms
81 catalyze the same reaction of converting acetyl-CoA to malonyl-CoA, but ACC1 is
82 located in the cytosol and is proposed to provide the pool of malonyl-CoA for fatty
83 acid synthesis, while ACC2 is located at the mitochondrion and is proposed to provide
84 the pool of malonyl-CoA that inhibits carnitine:palmitoyl-CoA acyl transferase-1
85 (CPT1) and hence the uptake and subsequent oxidation of fatty acids in
86 mitochondria[31-33]. Therefore, AMPK can both inhibit fatty acid synthesis by
87 phosphorylating ACC1 and promote fatty acid oxidation by inhibiting ACC2[34].
88 AMPK also phosphorylates the endoplasmic reticulum-localized form of the

89 transcription factor sterol regulatory element-binding protein-1c (SREBP-1c) at
90 Ser372, to inhibit its proteolytic cleavage and thereby suppress fatty acid synthesis at
91 the transcriptional level[35], while also inhibiting other anabolic pathways such as
92 glycogen, rRNA and nucleotide synthesis[34, 36], and inhibiting mTORC1 by
93 phosphorylating its upstream negative regulator, tuberous sclerosis complex-2
94 (TSC2)[37], and/or the mTORC1 subunit RAPTOR[38]. Interestingly, when cells are
95 facing shortage of glucose, the lysosomal v-ATPase and Ragulator complex becomes
96 involved in AMPK activation and dissociates mTORC1 from the lysosomal surface,
97 providing another level of inhibitory regulation of mTORC1[39, 40]. Apart from blocking
98 anabolic processes, AMPK stimulates various catabolic processes including glucose
99 uptake and autophagy. For example, it phosphorylates TBC1D1 to promote glucose
100 uptake in skeletal muscle[41, 42]. AMPK also directly phosphorylates ULK1 and
101 Beclin-1 at multiple sites to initiate autophagy under energy stress[43-45]. The
102 mitochondrial outer membrane-localized mitochondrial fission factor (MFF), which
103 promotes mitochondrial fragmentation prior to mitophagy, is also a direct substrate of
104 AMPK, thus leading to induction of mitophagy[46, 47]. Moreover, recent evidence has
105 indicated that AMPK is also localized in the nucleus, phosphorylating ten-eleven
106 translocation protein 2 (TET2)[48, 49].
107
108 In this study, we systemically evaluated how compartmentalized pools of AMPK are
109 regulated, and how different subcellular targets of AMPK are phosphorylated in
110 response to different severities of nutrient or energy stress. Emphasis was placed on

111 the dependency of AMPK activation on increases in cellular AMP, and AXIN1 as the
112 scaffold for the upstream kinase LKB1. We demonstrate that in MEFs starved for
113 glucose or livers of mice starved for 16 hr, when AMP:ATP or ADP:ATP ratios
114 remained unchanged, AMPK activation occurred exclusively in the lysosomal pool.
115 At medium-to-high AMP levels, as seen in HEK293 cells starved for glucose, or in
116 MEFs undergoing early phases of severe nutrient starvation (removal of both glucose
117 and glutamine from the medium), cytosolic as well as lysosomal AMPK is activated,
118 but AXIN1 is still needed to promote LKB1-AMPK association. By contrast, when
119 cellular AMP levels are elevated to high levels due to severe nutrient starvation or
120 ischemia, mitochondrial AMPK becomes activated independently of AXIN1,
121 presumably via conformational changes in AMPK that allow LKB1 to directly
122 phosphorylate Thr172. Importantly, we found that AXIN2 (also known as AXIL or
123 Conductin), which shows redundancy with AXIN1 in Wnt signaling[50], can also
124 functionally replace AXIN1 in bridging LKB1 and AMPK. This spatiotemporal
125 regulation of AMPK complexes in different compartments may be due to expression
126 of different combinations of subunit isoforms, and may have profound physiological
127 and pharmacological implications.
128
129 **RESULTS**
130 **Basal AMP is sufficient for activation of the lysosomal pool of AMPK**
131 We previously showed that genetic knockout of either *AXIN1* or *LAMTOR1*, critical
132 components of the lysosomal AMPK activation complex, blocked AMPK activation

(assessed by phosphorylation of Thr172) in mouse embryo fibroblasts (MEFs) deprived of glucose[18]. We also reported that AMPK activation under these conditions was rapid (within 10 minutes) and was not accompanied by any increases in cellular AMP:ATP or ADP:ATP ratios[14]. However, we also found that more severe nutrient stress, caused by removal of both glucose and glutamine, caused a delayed activation of AMPK (up to 2 hr) that was independent of AXIN1 or LAMTOR1[14]. These results suggested that glucose starvation may exclusively activate the lysosomal pool of AMPK, whereas complete nutrient withdrawal may activate non-lysosomal pools. To address this, we optimized methods to perform subcellular fractionation in MEFs (validation shown in Supplementary information, Fig. S1a-c) and systematically determined which pools of AMPK (cytosolic, lysosomal, mitochondrial, and nuclear) are activated by glucose deprivation. As shown in Fig. 1a and Supplementary information, Fig. S1d, Thr172 phosphorylation was only detected in the lysosomal fraction, but not in cytosolic, mitochondrial or nuclear fractions from MEFs cultured in low glucose (5 mM or below), in which AMP:ATP and ADP:ATP ratios were unchanged (Fig. 1b). Similar results were obtained in HEK293T cells (Supplementary information, Fig. S1e, f). Subcellular fractionation of liver homogenates from mice starved for 16 hr, which showed no changes in adenine nucleotide ratios, also indicated that Thr172 phosphorylation was only detected in the lysosomal fraction (Fig. 1c, d). Interestingly, we found that under these conditions phosphorylation of ACC1, but not ACC2, was increased (Fig. 1e, f; Supplementary information, Fig. S1g). Increased phosphorylation at the AMPK sites on SREBP1c, TSC2, Raptor and

155 HDAC4, but not MFF, also occurred (Fig. 1g). These data suggest that inhibition of
156 synthesis of lipid, protein and carbohydrates is an early event during the response to
157 glucose starvation, and occurs prior to any energy stress. In addition, phosphorylation
158 of Ser660 of TBC1D1 involved in glucose uptake was also detected after glucose
159 starvation, indicating an immediately early pro-catabolic activity (Fig. 1g).
160
161 It has been well established that AXIN2, which shares the RGS and DIX domains as
162 well as the binding sites for β-catenin, GSK3, Diversin, and Smad3, is functionally
163 equivalent to AXIN1, although AXIN2 is not expressed ubiquitously like AXIN1 but
164 instead in tissue- and developmental-stage-specific patterns[50, 51]. In the course of
165 testing for the generality of the mechanisms linking glucose sensing to AMPK
166 activation in various cell lines, we observed that AMPK was still activated by glucose
167 starvation in HEK293T cells even when *AXIN1* was knocked down (Fig. 1h).
168 However, AXIN2 was expressed at a readily detectable level in these cells, compared
169 to MEFs, HEK293 cells, and the liver (Supplementary information, Fig. S1h, i),
170 implying that in HEK293T cells AXIN2 was compensating for AXIN1 when the latter
171 was knocked out or knocked down. Moreover, knockdown of *AXIN1* in HEK293T
172 cells elevated the levels of AXIN2 (Supplementary information, Fig. S1h). We also
173 knocked down *AXIN1* in *AXIN2*$^{-/-}$ HEK293T cells, and found that the activation of
174 AMPK by glucose starvation was indeed largely abrogated (Fig. 1h). Similarly,
175 introduction of AXIN2 into *AXIN1*$^{-/-}$ MEFs (in which AXIN2 was almost
176 undetectable) led to a significant activation of AMPK upon glucose starvation (Fig.

177 1i). In conclusion, our results supported that AXIN1 and AXIN2 are functionally
178 equivalent in the lysosomal pathway of AMPK activation.
179
180 **Modest increases in AMP activate cytosolic AMPK in an AXIN1-dependent**
181 **manner**
182 Surprisingly, unlike in MEFs or mouse liver[18], in HEK293 cells in which *LAMTOR1*
183 was knocked down activation of AMPK by glucose starvation was still observed (Fig.
184 2a). To reconcile these differences, we performed subcellular fractionation assays in
185 HEK293 cells and found that LAMTOR1-independent activation of both cytosolic
186 and lysosomal AMPK, which was blocked when *AXIN1* was knocked down, was
187 observed (Fig. 2b). This evoked previous findings that there were modest increases in
188 AMP/ATP and ADP/ATP ratios in HEK293 cells upon glucose removal[14], suggesting
189 that AXIN1 can also act as a bridge that tethers AMPK and LKB1 in the cytosol when
190 AMP is modestly elevated[19]. In this study, cellular AMP was increased in response to
191 glucose removal from 30 μM to 60 μM, with an increase in AMP/ATP ratio from
192 0.006 to 0.015 (Fig. 2c), similar to extents observed in MEFs undergoing early phases
193 of severe starvation[14]. Under these conditions, AMPK phosphorylated ACC1 and
194 ACC2 in a similar manner to that seen in MEFs upon glucose starvation (Fig. 2d;
195 Supplementary information, Fig. S2a). We also used AICAR to mimic a moderate
196 increase in AMP in MEFs. MEFs treated with 0.6 mM AICAR yielded an estimated
197 intracellular ZMP concentration of 1.2 mM which, given that ZMP is about 40-fold
198 less potent than AMP for AMPK activation[52], is equivalent to around 50 μM AMP (in

addition to about 20 μM endogenous AMP), similar to the concentration estimated in HEK293 cells upon glucose starvation (Supplementary information, Fig. S2b). Consistently, we found an AXIN1-dependent, LAMTOR1-independent activation of both lysosomal and cytosolic AMPK, similar to that observed in HEK293 cells (Fig. 2e-h; Supplementary information, Fig. S2c, d). Taken together, these results suggested that AXIN1 also participates in the activation of cytosolic AMPK when AMP levels are moderately increased.

To further confirm that AXIN1 can play a role in bridging LKB1 to AMPK in the activation of cytosolic AMPK as well as in the lysosomal pathway, we observed that in both lysosomal and cytosolic fractions, the increased LKB1-AMPK interaction induced in conditions that caused elevation of AMP to moderate levels was dampened in the absence of AXIN1 (Fig. 2i). In vitro reconstitution experiments showed that addition of a moderate level of AMP (60 μM) significantly promoted the phosphorylation of AMPK by LKB1 in vitro in an AXIN1-dependent manner (Supplementary information, Fig. S2e). Taken together, these results demonstrate that after moderate elevation of AMP, AXIN1 alone can tether LKB1 to AMPK without the necessity for the v-ATPase-Ragulator complex involved in the lysosomal pathway.

The mitochondrion-localized ACC2 is phosphorylated by AMPK only after severe nutrient stress

We next analyzed the regulation of AMPK and its substrates under severe nutrient stress. When MEFs were severely starved or treated with 2 mM AICAR (yielding 3.6 mM intracellular ZMP, equivalent to around 110 μM AMP (in addition to around 20 μM endogenous AMP), mimicking the levels of AMP accumulated under severe nutrient stress), full activation of AMPK in the cytosolic, lysosomal and mitochondrial pools was observed (Fig. 3a, b). Such a full phosphorylation of AMPK was also observed in HEK293 and HEK293T cells (Fig. 2a, b; Supplementary information, Fig. S1e). Of note, no nuclear AMPK activation could be detected in any level of stress (Supplementary information, Fig. S1d). Under these conditions, we found that ACC2 was phosphorylated as well as ACC1 (Fig. 3C). Compared with ACC1, ACC2 has an additional N-terminal hydrophobic sequence that specifically targets it to the mitochondrial outer membrane[31] (also validated in Supplementary information, Fig. S3a-c). We thus probed the p-ACC signals in cytosolic and mitochondrial fractions, and found that the mitochondrial p-ACC could only be detected under conditions of severe nutrient stress (Fig. 3d). To obtain unequivocal evidence that the p-ACC signals seen after severe nutrient stress was contributed by ACC2, we generated *ACC1*$^{-/-}$ and *ACC2*$^{-/-}$ MEFs (Fig. S3d). Knockout of *ACC2*, unlike that of *ACC1*, had no effect on the phosphorylation of ACC upon glucose starvation or after a moderate elevation of AMP, but blocked the increase of the p-ACC signal in severe nutrient stress (Fig. 3e). Moreover, we found that levels of malonyl-CoA were decreased by 50% in MEFs starved for glucose only, and were further decreased by up to 90% under severe nutrient starvation, to a similar extent as

243 the reduction caused by treatment with TOFA (a pan-ACC inhibitor), without any
244 significant change on its precursor, acetyl-CoA (Fig. 3f). Consistently, both ACC1
245 and ACC2, along with AMPK from all the fractions, were phosphorylated in liver of
246 mice subjected to hepatic ischemia, when a large, 22-fold increase of AMP:ATP ratio
247 was detected (equivalent to an increase of AMP from 20 μM to 475 μM, estimated as
248 described previously[53], Fig. 3g, h; Supplementary information, Fig. S3e); a further
249 decrease of malonyl-CoA, compared with that seen after 16-hr starvation, was also
250 observed (Fig. 3i). We found that when there were large increases in AMP, knockout
251 of *AXIN1* or *LAMTOR1* did not block the phosphorylation of ACC1, ACC2 or AMPK
252 in either the cytosolic, lysosomal or mitochondrial fractions (Supplementary
253 information, Fig. S3f-i).
254
255 ACC1 and ACC2 contain very similar AMPK substrate recognition motifs[54] (which is
256 why phospho-specific antibodies recognize both), but vary in their subcellular
257 locations. We hypothesized that the targets of AMPK may be regulated in a
258 spatiotemporal manner under different stress conditions. To test this, we replaced the
259 endogenous AMPK-β subunits with modified forms that target the complex to
260 specific locations. It is known that N-myristoylation is required for AMPK association
261 with intracellular membranes such as the lysosome[14] and the mitochondrion[24]. We
262 generated two fusion constructs with modifications at the N-terminus of the β1
263 subunit: either adding the LAMP2 (for tethering to the lysosomal surface, referred to
264 as lyso-β1), or TOMM20 (for tethering to mitochondrial outer membrane, referred to

as mito-β1), and also the β1-G2A mutation (preventing N-myristoylation, referred to as cyto-β1) (diagrammed in Fig. 3j). Before reintroduction of the engineered constructs to cells, we knocked out the β subunits (β1 and β2) of AMPK in HEK293T cells, generating AMPKβ-DKO cells (validation in Supplementary information, Fig. S4a). Lyso-β1, mito-β1 and cyto-β1 were then individually re-introduced to the AMPKβ-DKO cells. As shown in Supplementary information, Fig. S4b, the engineered β1 subunits assembled into heterotrimeric AMPK complexes like the wild-type AMPK-β1, and were successfully localized as expected, as validated by immunostaining (Supplementary information, Fig. S4c). We next treated the cells with A-769662, a β1-specific activator[55], to cause a compartmentalized activation of AMPK (validated in Supplementary information, Fig. S4d). We found that in lyso-β1-expressing cells, only cytosol-localized ACC1 can be phosphorylated in response to A-769662 treatment (Fig. 3k). By contrast, in mito-β1- and cyto-β1-expressing cells, both the cytosol-localized ACC1 and the mitochondrion-localized ACC2 were phosphorylated (Fig. 3k). Therefore, mitochondrion-localized ACC2 seems to be specifically phosphorylated under severe nutrient stress, in which mitochondrial and cytosolic AMPK are also fully activated. Supporting this, we found that the mitochondrial fission factor MFF, another well-characterized mitochondrion-localized AMPK substrate[47], was phosphorylated in a similar manner to ACC2 (Fig. 1g).

Roles of AMP in the hierarchical activation of AMPK

We postulated that upon starvation for glucose only, basal AMP might act as a necessary cofactor for AMPK activation via the lysosomal pathway, while elevated AMP may bind to additional sites on AMPK. Indeed, when the AMPK-γ1 mutant D317A, which affects the "non-exchangeable" site for AMP (site 4), was re-introduced into HEK293T cells with all γ subunits (γ1 to γ3) knocked out (AMPKγ-TKO, generated as shown in Supplementary information, Fig. S4e), activation of AMPK upon glucose starvation was severely dampened (Fig. 4a), consistent with our previous finding that the AMP-promoted interaction between LKB1 and AMPK was impaired by this mutant[19]. We also introduced the R531G mutant, in which the exchangeable site for AMP (site 3[8]) is disrupted, into AMPKγ-TKO cells, and found that the phosphorylation of lysosomal AMPK upon glucose starvation remained unaffected, whereas the cytosolic and mitochondrial AMPK phosphorylation under moderate and high AMP levels was blocked (Fig. 4b). Similarly, phosphorylation of ACC2 was blocked in the R531G-expressing cells (Fig. 4c). We also determined whether it is indeed AMP itself that mediated such effects by knocking out adenylate kinase 1 (AK1, which catalyzes the conversion of 2 ADP to 1 ATP and 1 AMP) in MEFs (Supplementary information, Fig. S4f). Indeed, we found that knockout of *AK1* significantly dampened the activation of mitochondrial- and cytosolic-localized AMPK, and the phosphorylation of ACC2 under severe nutrient stress (Fig. 4d; Supplementary information, Fig. S4g).

DISCUSSION

In this study, we have systemically determined how the differentially localized AMPK complexes are regulated to affect distinct target phosphorylation in response to different stresses (Fig. 4e). Under conditions of glucose starvation that did not elevate cellular AMP:ATP or ADP:ATP ratios, only lysosomally localized AMPK was activated, exclusively through the lysosomal pathway. However, when AMP was moderately elevated, cytosolic AMPK was also activated in addition to lysosomal AMPK. Activation induced by moderate increases in AMP was not mediated via the lysosomal pathway, because knockout of *LAMTOR1* (a subunit of the Ragulator complex) had no effect, although activation was still dependent on AXIN1. In support of this, moderately elevated AMP promoted the formation of a complex between AXIN1, LKB1 and AMPK. Interestingly, mitochondrial AMPK was not activated by moderate increases in AMP, but only in response to more severe nutrient stress when there were larger increases in AMP. One possible explanation for this is that the concentrations of ATP are higher in the vicinity of mitochondria, inhibiting the activation of AMPK by AMP. However, when cellular AMP is elevated to higher levels during severe nutrient stress or ischemia, mitochondrial AMPK becomes activated independently of AXIN1, phosphorylating the mitochondrially localized substrates, ACC2 and MFF.

Basal AMP is believed to be maintained at low levels by the freely reversible adenylate kinase reaction (2ADP ↔ ATP + AMP), with the high ATP:ADP ratio in unstressed cells driving the reaction from right to left, i.e. towards ADP and away

331 from AMP. AMP is thought to be constantly bound as a cofactor to site 4 of the
332 AMPK-γ subunit[7, 8], perhaps rendering the AMPK complex ready for activation
333 through the aldolase-v-ATPase-Ragulator pathway when glucose runs low. Although
334 AXIN is required for activation of both lysosomal and cytosolic AMPK, increases in
335 AMP are required for activation of cytosolic AMPK. A possible explanation for this is
336 that the presence of Ragulator and v-ATPase on the lysosome alters the conformation
337 of the intrinsically disordered protein AXIN that can form various intramolecular
338 loops[56, 57], such that it is more accessible to AMPK even at basal levels of AMP. By
339 contrast, in the cytosol, AXIN does not come into contact with the
340 Ragulator:v-ATPase complex, so that only when AMP is bound at a site additional to
341 site 4 (most likely site 3, supported by the results obtained using the R531G mutant)
342 which likely causes conformational changes therein[58, 59], AXIN and LKB1 forms a
343 complex with cytosolic AMPK. Finally, when cells are subjected to severe nutrient
344 stress, AMP is increased to such high levels that AMPK is fully occupied by AMP,
345 and LKB1 does not require AXIN to bind AMPK.
346
347 AMPK is composed of three subunits, each occurring as more than one isoform (α1,
348 α2; β1, β2; γ1, γ2, γ3). These isoforms, some of which are expressed in a
349 tissue-specific manner, can form up to twelve different heterotrimeric combinations[60].
350 It has been proposed that these different isoform combinations target AMPK to
351 different subcellular locations[3, 61, 62]. Indeed, studies have shown that isoform-specific
352 activations of AMPK lead to different effects on metabolic controls. For example,

353 compared to AICAR, A-769662 (the β1-specific activator) only mildly stimulated
354 fatty acid oxidation, although robustly inhibited fatty acid synthesis[63]. The AMPK
355 complex containing the γ1-D317A mutant showed strong preference for cytosolic
356 presence[64], and failed to stimulate fatty acid oxidation despite its chronic activity[65].
357 Based on the results in this paper, it is conceivable that different thresholds of stress
358 are involved in triggering differentially localized AMPK heterotrimers, and that
359 different heterotrimeric AMPK complexes might have specificity for targets due to
360 different subcellular locations. Indeed, it is already known that AMPK complexes
361 containing γ1, γ2 and γ3 differ in their sensitivity to activation by AMP and ADP[9].
362
363 Our current study has shown that an immediate role of AMPK activation is to
364 phosphorylate and inhibit factors involved in anabolic pathways including ACC1,
365 SREBP1c, HDAC4, TSC2, and Raptor. It is interesting that ACC2 is phosphorylated
366 only under conditions of more severe nutrient stress and ischemia, when there are
367 larger increases in AMP. This indicates that fatty acid oxidation, a catabolic pathway,
368 is increased during more severe stress, while fatty acid synthesis is shut down during
369 a mild stress, i.e. lack of glucose. Since glucose is a major precursor for fatty acid
370 synthesis in many cell types, it might make sense for this pathway to be switched off
371 when there is reduced availability of glucose. By contrast, ACC2 appears to be
372 phosphorylated only under conditions of more severe nutrient stress (lack of both
373 glucose and glutamine), when fatty acid oxidation may need to be facilitated as an
374 alternate energy source. It is also interesting to note that ULK1 and Beclin-1 become

375 phosphorylated at an early stage of glucose starvation[44], exactly the time point that
376 AMPK is activated[14], although autophagy takes place only at a later stage in which
377 additional factors such as accumulated ammonia, and the increased acetylation of
378 VPS34 are involved in the formation of autophagosomes[66, 67]. Consistently, we also
379 showed that the mitochondrial fission factor MFF, which promotes the formation of
380 fragmented mitochondria prior to mitophagy/autophagy is only phosphorylated after
381 severe starvation. Taken together, differently localized AMPK pools are differentially
382 regulated, with AMP-dependent and AMP-independent pathways operating in a
383 spatiotemporal manner. Our paper supports the view that glucose sensing by the
384 lysosomal AMPK activation pathway serves to act as a surveillance system
385 monitoring the availability of glucose and switching off anabolic pathways, many of
386 which require glucose for the provision of precursors. We also suggest that
387 pharmacological activation of all pools of AMPK might have adverse effects on
388 cellular and tissue physiology, and that new strategies may be required to activate the
389 appropriate spatial and temporal pools of AMPK in order to develop effective and
390 safe drugs for treating metabolic diseases.
391
392 Although we have demonstrated that different severities of nutritional stress modulate
393 different pools of AMPK and different downstream targets, contingent on different
394 cellular levels of AMP, in some cases it remains unclear how this relates to the
395 physiological roles of the targets. For example, we found that ACC2 is
396 phosphorylated only after severe nutrient stress in MEFs, and is not phosphorylated in

liver even from overnight-starved mice. However, fatty acid oxidation has been reported to be enhanced in mice that were starved overnight[68]. Thus, elevated fatty acid oxidation under mild starvation may be caused by processes other than ACC2 phosphorylation. Indeed, it has been reported that increased circulating fatty acid, released primarily by adipose tissues[69], and enhanced expression of CPT1[70], may be involved under these circumstances. Another interesting issue is that ULK1 and Beclin-1 are among the substrates that are phosphorylated by AMPK immediately after glucose starvation, yet autophagy does not take place upon short-term glucose starvation. It therefore remains unclear what the roles of the phosphorylation of ULK1 and Beclin-1 by AMPK exert beyond autophagy, although ULK1/2 have been shown to play a role in modulating glucose metabolic fluxes, independently of autophagy[71].

MATERIALS AND METHODS

Antibodies

Rabbit polyclonal antibody against LAMTOR1 was raised and validated as described previously[18], and was diluted 1:100 for immunoprecipitation (IP) or 1:500 for immunoblotting (IB). Rabbit anti-phospho-AMPKα-T172 (cat. #2535, 1:1000 for IB), anti-AMPKα (cat. #2532, 1:1000 for IB), anti-phospho-ACC-Ser79 (cat. #3661, 1:1000 for IB), anti-ACC (cat. #3662, 1:1000 for IB), anti-LKB1 (cat. #3047, 1:1000 for IB), anti-AMPKβ1/2 (cat. #4150, 1:1000 for IB), anti-AMPKγ1 (cat. #4187, 1:1000 for IB), anti-AMPKγ2 (cat. #2536, 1:1000 for IB), anti-AMPKγ3 (cat. #2550, 1:1000 for IB), anti-AXIN1 (cat. #2074, 1:1000 for IB), anti-AXIN2 (cat. #2151,

1:1000 for IB), anti-ACC1 (cat. #4190, 1:1000 for IB and 1:100 for IP), anti-ACC2 (cat. #8578, 1:1000 for IB and 1:25 for IP), anti-phospho-SREBP1c-S372 (cat. #9874, 1:500 for IB), anti-phospho-Raptor-S792 (cat. #2083, 1:1000 for IB), anti-Raptor (cat. #2280, 1:1000 for IB), anti-phospho-TSC2-S1387 (cat. #2280, 1:1000 for IB), anti-TSC2 (cat. #4308, 1:1000 for IB), anti-phospho-HDAC4-S246 (cat. #3443, 1:1000 for IB), anti-HDAC4 (cat. #7628, 1:1000 for IB), anti-phospho-MFF-S146 (cat. #49281, 1:500 for IB), anti-MFF (cat. #86668, 1:1000 for IB), andi-phospho-TBC1D1-S660 (cat. #6928, 1:500 for IB), anti-TBC1D1 (cat. #4629, 1:1000 for IB), anti-phospho-ULK1-S555 (cat. #5869, 1:1000 for IB), anti-phospho-Beclin-1-S93 (cat. #14717, 1:1000 for IB), anti-Beclin-1 (cat. #3495, 1:1000 for IB), anti-COXIV (cat. #4850, 1:1000 for IB and 1:200 for IF), anti-PDI (cat. #3501, 1:1000 for IB), anti-Lamin B1 (cat. #13435, 1:1000 for IB), anti-β-tubulin (cat. #2128, 1:1000 for IB), anti-HA-tag (cat. #3724, 1:200 for IF), mouse anti-Myc-tag (cat. #2276, 1:1000 for IB), and HRP-conjugated mouse anti-rabbit IgG (conformation specific, cat. #5127, 1:2000 for IB) antibodies were purchased from Cell Signaling Technology. Rabbit anti-AK1 (cat. 14978-1-AP, 1:500 for IB) and rabbit anti AXIN2 (cat. 20540-1-AP, 1:1000 for IB, only for Supplementary information, Fig. S1h) were purchased from Proteintech. Mouse anti-LAMP1 (cat. ab13523, 1:200 for IF), anti-AMPKα (cat. ab80039, 1:100 for IP) and rat anti-LAMP2 (cat. ab13524, 1:1000 for IB) were purchased from Abcam. The ANTI-FLAG® M2 Affinity Gel (cat. A2220) and rabbit anti-ULK1 (cat. A7481, 1:1000 for IB) were purchased from Sigma. Goat anti-AXIN (cat. sc-8567, 1:100 for

IP and 1:60 for IF), rabbit anti-SREBP1 (cat. sc-366, 1:1000 for IB), and mouse anti-HA (cat. sc-7392, 1:2000 for IB and 1:200 for IF) antibodies were purchased from Santa Cruz Biotechnology. The HRP-conjugated goat anti-mouse IgG (cat. 115-035-003, 1:5000 for IB) and HRP-conjugated goat anti-rabbit IgG (cat. 111-035-003, 1:5000 for IB) antibodies were purchased from Jackson ImmunoResearch.

Bacterial and virus strains

Stbl3 (cat. C737303, for transformation of pBOBI- and pLL3.7-based constructs), BL21 (DE3, cat. C600003, for transformation of pET-based constructs) and DH5α (cat. 18258012, for transformation of other constructs) competent cells were purchased from Thermo Fisher Scientific.

Chemicals and recombinant proteins

TOFA (cat. sc-200653A) was purchased from Santa Cruz Biotechnology. AICAR (cat. A9978), AMP (cat. 01930) and LKB1 complex (cat. SRP0246) were purchased from Sigma. A-769662 (cat. S2697) was purchased from Selleck. Lysosome Isolation Kit (cat. LYSISO1) was purchased from Sigma.

Cell lines

HEK293T cells (cat. CRL-3216) were obtained from ATCC, and HEK293 cells (cat. CRL-1573) were obtained from Invitrogen. *LAMTOR1*$^{F/F}$or *AXIN*$^{F/F}$ MEFs were

established by introducing SV40 T antigen into primary cultured embryonic cells from a litter of corresponding mice.

Oligonucleotides

The siRNAs against human AXIN1 and LAMTOR1 were constructed and validated as described previously[18, 19]. The sequence for each sgRNA is as follows (forward strand only):

5'- TAGGATCGGAAACTTACTAGTGG -3' and 5'- GGCTCAGGTTAACTAACGT TAGG -3' for human *PRKAB1*,

5'- TTTAGGCAGTGCTTGAGCATAGG -3' and 5'- CGGCCACTTAGTATATCTGT GGG -3' for human *PRKAB2*,

5'- CTGATTTATAGTAGCGGTGCAGG-3' for human *PRKAG1*,

5'- GATGCAGTCACTCCACGCTCTGG -3' and 5'- CGGTGGCACCGAAGCTGC CAGG-3' for human *PRKAG2*,

5'-AGCCCGTGCGCTCAATCTTCTGG-3' and 5'-TGGGGCCTGTTTGGTTAATA GGG-3' for human *PRKAG3*,

and 5'-CACCGAGTCAGCTCTGGATCGGAGA-3' for mouse *Ak1*.

Animals

AXIN$^{F/F}$, *LAMTOR1*$^{F/F}$ mice were generated and maintained as described[18].

ACC1-floxed mouse (Stock No. 030954, The Jackson Laboratory) was a generous gift from Prof. Jay Horton (UT Southwestern Medical Center), and the *ACC2*$^{-/-}$ mouse from Prof. Tian Xu (Institute of Developmental Biology and Molecular Medicine, Fudan University). Wildtype C57BL/6J mice were purchased from Beijing Vital River Laboratory Animal Technology Co., Ltd., and were housed at Animal Core Facility. Male littermate mice of 6-week old were used in this study. Mice were housed with free access to water and standard diet (65% carbohydrate, 11% fat, 24% protein). Protocols for all animal experiments were approved by the Institutional Animal Care and the Animal Committee of Xiamen University.

Mouse studies

For starvation, the diet was withdrawn from the cage at 5 p.m. and mice were sacrificed at 9 a.m. the next day by cervical dislocation. For hepatic ischemia, a surgery was performed as described previously[72], with some modifications. Mice were anesthetized with pentobarbital sodium solution (100 mg/kg) by intraperitoneal injection and were placed on a heating plate set at 37 °C. Mouse abdomen was gently opened (from the mid-abdomen to the xiphoid) to expose the liver, and its intestine was covered by moisten gauze to prevent from drying. The portal vein, hepatic artery, and bile duct were then cross-clamped by an atraumatic clip at a place just above the branching to the right lateral lobe to subject the median and the left lateral lobes to ischemia. Mice that went through same surgery but did not undergo cross-clamping on blood vessel and bile duct were considered as sham. Unless stated otherwise, liver

507 tissues were dissected and instantly frozen in liquid nitrogen for immunoblotting, and
508 were freeze-clamped for metabolites extraction and fractionation.
509
510 **Plasmids**
511 Point mutations on AMPK-γ1 (D317A), AMPK-γ2 (R531G) and AMPK-β1 (G2A)
512 were performed by a PCR-based site-directed mutagenesis method using PrimeSTAR
513 HS polymerase (Takara). Expression plasmids for various proteins were constructed
514 in the pcDNA3.3 vector for transient transfection (ectopic expression), in pBOBI for
515 lentivirus packaging (stable expression). PCR products were verified by sequencing
516 (Invitrogen, China). The lentivirus-based vector pLL3.7 was used for expression of
517 siRNA in HEK293T and HEK293 cells.
518
519 **CRISPR/Cas9 knockout cell lines**
520 Genes were deleted in HEK293T cells (human *PRKAB1*, *PRKAB2*, *PRKAG1*,
521 *PRKAG2*, and *PRKAG3*) or MEFs (mouse *Ak1*) using the CRISPR-Cas9 system.
522 Targeting nucleotides were designed using http://crispr.mit.edu. Oligonucleotides of
523 human PRKAG1 were inserted into pX260 vector, human PRKAB1, PRKAB2,
524 PRKAG2, and PRKAG3 into pX330 vector, and mouse AK1 into lentiCRISPRv2
525 vector. The individual constructs were then subjected to transfection of HEK293T
526 cells (pX260 and pX330) followed by single-cell sorting into 96-well dishes, or
527 lentivirus packaging (lentiCRISPRv2) using HEK293T cells. In both conditions, cells
528 were transfected with 3 μg of DNA with Lipofectamine 2000 (Invitrogen, Cat.

11668-027) per well of a 6-well plate. Clones were expanded and evaluated for knockout status by sequencing.

Cell culture, transient transfection and lentivirus Infection

HEK293T, HEK293 and MEFs were maintained in Dulbecco's modified Eagle's medium (DMEM, Gibco, cat. 11965) supplemented with 10% fetal bovine serum (FBS), 100 IU penicillin, 100 mg/ml streptomycin at 37 °C in a humidified incubator containing 5% CO_2. Polyethylenimine (Polysciences, Inc., Cat. #23966) at a final concentration of 10 μM was used to transfect HEK293T cells. Total DNA for each plate was adjusted to the same amount by using relevant empty vector. Transfected cells were harvested at 24 hr after transfection. Lentiviruses for infection of the MEFs were packaged in HEK293T cells using Lipofectamine 2000 transfection. At 30 hr post transfection, medium was collected and added to the cells. The cells were incubated for another 24 hr. *LAMTOR1*$^{F/F}$or *AXIN*$^{F/F}$ MEFs were established by introducing SV40 T antigen into primary cultured embryonic cells from a mouse litter. *LAMTOR1*$^{-/-}$ or *AXIN*$^{-/-}$ MEFs were generated by infecting *LAMTOR1*$^{F/F}$ or *AXIN*$^{F/F}$ MEFs with adenovirus expressing Cre recombinase for 12 hr. The infected cells were then incubated in fresh DMEM for another 8 to 10 hr before further treatments. Cells were verified to be free of mycoplasma contamination and authenticated by STR sequencing.

For glucose starvation, cells were rinsed twice with PBS, and then incubated in glucose-free DMEM (Gibco, cat. 11966) supplemented with 10% FBS and 1 mM

sodium pyruvate (Gibco, cat. 11360) for desired periods of time at 37 °C. For starvation for glucose plus glutamine, cells were incubated in DMEM with 5 mM glucose overnight, and then incubated for desired periods of time in fresh DMEM lacking glucose, glutamine, phenol red or pyruvate (Gibco cat. A14430-01), in which 1 mM pyruvate was added, with or without Glutamax™ (Gibco cat. 35050-038) and D-glucose (Gibco cat. A2494001), all without FBS.

Subcellular fractionation.

All buffers used for subcellular fractionation contains protease inhibitor cocktail (Sigma, cat. P8340).

Lysosomes were purified by Lysosome Isolation Kit according to the manufacturer's instructions, with minor modifications. Briefly, cells from sixty 10-cm dishes (60-80% confluence) were collected by direct scrapping at room temperature, followed by centrifugation for 5 min at 500 *g* at 37 °C. Cells were resuspend in 7 ml of 1× Extraction Buffer at room temperature. For isolating lysosomes from mouse livers, some 500 mg of frozen liver tissue was directly homogenized in 7 ml of ice-cold 1× Extraction Buffer. The cells/liver homogenates were then dounced in a 7-ml Dounce homogenizer (Sigma, cat. P0610) for 120 strokes on ice followed by centrifuging for 10 min at 1,000 *g*, 4 °C, yielding post-nuclear supernatants (PNS). The PNS were then centrifuged for 20 min at 20,000 *g* and the pellets were suspended in 1× Extraction Buffer by gentle pipetting, generating Crude Lysosomal Fractions (CLF). The volume of CLF was adjusted to 2.4 ml and then equally divided into six 1.5 mL

573 Eppendorf tubes (400 μl per tube). 253 μl of OptiPrep and 137 μl of 1× OptiPrep
574 Dilution Buffer were added to each CLF, and mixed by gentle pipetting. The mixtures
575 were defined as the Diluted OptiPrep Fraction (DOF). Each DOF (0.8 ml) was loaded
576 onto an 11 × 60 mm centrifuge tube at the top of 27% (0.4 ml) and 22.5% (0.5 ml)
577 OptiPrep solution cushions, and then overlaid with 16% (1 ml), 12% (0.9 ml) and 8%
578 (0.3 ml) OptiPrep solutions. The tubes were then centrifuged on a SW60 Ti rotor
579 (Beckman) at 150,000 *g* for 4 hr at 4 °C, and the fractions at the top of 12% OptiPrep
580 solution were collected as the crude lysosome fractions. The fractions were diluted
581 with two volumes of PBS, followed by centrifugation at 20,000 *g* for 20 min. The
582 sediment was the lysosome fraction.
583 Mitochondria were purified as described previously[73], with minor modifications.
584 Briefly, forty 10-cm dishes of regularly cultured, severely starved or AICAR-treated
585 cells (60-80% confluence), or sixty 10-cm dishes of glucose-starved cells were
586 collected by direct scrapping at room temperature, followed by centrifugation for 5
587 min at 500 *g* at 37 °C. Cells were then resuspended in 20 ml of ice-cold IB_{cells}-1
588 buffer (225 mM mannitol, 75 mM sucrose, 0.1 mM EGTA and 30 mM Tris-HCl, pH
589 7.4). For isolating mitochondria from mouse livers, some 500 mg of frozen liver was
590 directly homogenized in 10 ml of IB_{liver}-1 buffer (225 mM mannitol, 75 mM sucrose,
591 0.5% BSA, 0.5 mM EGTA and 30 mM Tris-HCl, pH 7.4). Cells or liver homogenates
592 were then dounced in a 40-ml Dounce homogenizer (Sigma, cat. D9188) for 100
593 strokes, followed by two times of centrifugation for 5 min at 600 *g* (for cells) or 740 *g*
594 (for liver tissues) at 4 °C. The supernatants were then collected and centrifuged for 10

min at 7,000 *g* (for cells) or 9,000 *g* (for liver tissues) at 4 °C. The pellets were then washed with 20 ml of ice-cold IB_{cells}-2 buffer (for cells, 225 mM mannitol, 75 mM sucrose and 30 mM Tris-HCl pH 7.4) or ice-cold IB_{liver}-2 buffer (for liver tissues, IB_{cells}-2 buffer supplemented with 0.5% BSA) twice. The suspensions were first centrifuged at 7,000 *g* (for cells) or 10,000 *g* (for liver tissues), and were centrifuged again at 10,000 *g*, both for 10 min at 4 °C. Note that for liver tissues, the pellets subjected to the second time of centrifugation were resuspended in 20 ml of ice-cold IB_{cells}-2. The pellets were then resuspended in 2 ml of ice-cold MRB buffer (250 mM mannitol, 5 mM HEPES pH 7.4 and 0.5 mM EGTA), and were loaded on top of 10 ml of Percoll medium (225 mM mannitol, 25 mM HEPES pH 7.4, 1 mM EGTA and 30% Percoll (v/v)) in 14 × 89-mm centrifuge tubes (Beckman, ref. 344059). Tube were then centrifuged on a SW41 rotor (Beckman) at 95,000 *g* for 0.5 hr at 4 °C, and the dense band located approximately at the bottom of each tube was collected. The collected fractions were diluted with 10 volumes of MRB buffer, followed by centrifugation at 6,300 *g* for 10 min at 4 °C, and washed with 2 ml of MRB buffer, followed with centrifugation at 6,300 *g* for 10 min at 4 °C. The pellets were pure mitochondria.

Cytosol was purified as described[74]. Briefly, some 0.15 g of each freshly excised liver tissue, or ten 10-cm dishes of cells were homogenized in 800 μl of the homogenization buffer (HB) containing 250 mM sucrose, 3 mM imidazole, pH 7.4. Homogenates were then passed through a 22-G needle attached to a 1-ml syringe for six times, and were then centrifuged at 2,000 *g* for 10 min to yield PNS. PNS samples

were then loaded on to the top of 11 × 60-mm centrifuge tubes that have been loaded sequentially with 1 ml of 40.6% sucrose (dissolved in HB), 1 ml of 35% sucrose (dissolved in HB), and 1 ml of 25% sucrose (dissolved in HB). Tubes were then centrifuged on an SW60 Ti rotor (Beckman) at 35,000 rpm for 1 hr at 4 °C, and the top fractions (about 200 μl) were collected as cytosolic fraction.

Fractionation of nucleus was performed as described previously[19]. Briefly, cells were homogenized in Buffer A (10 mM HEPES, pH 7.9, 10 mM KCl, 0.1 mM EDTA, 0.1 mM EGTA, and 0.15% NP-40) and placed in ice for 15 min. The homogenates were centrifuged at 12,000 *g* for 1 min at 4 °C. The pellets were washed three times with Buffer A and then resuspended in Buffer B (20 mM HEPES, pH 7.9, 0.4 mM NaCl, 1 mM EDTA, 1 mM EGTA, 0.5% NP-40) and sonicated at 4 °C. Cellular debris was removed by centrifugation at 12,000 *g* for 30 min at 4 °C, and the supernatant was nuclear fraction.

Protein production

AXIN1, and AMPK complexes were expressed and purified in *E. coli* as described previously[19]. Briefly, full length AXIN1 was cloned into pET32a vector and transformed into the *E. coli* strain BL21 (DE3). The transformed cells were induced with 0.1 mM IPTG at an optical density of 0.4 at 600 nm (for AMPK, to 1.0 at 600 nm). After growing for 4 hr at 16 °C (for AMPK, growing for 16 hr), the cells were collected, homogenized in a buffer (50 mM sodium phosphate, pH 7.4, 150 mM NaCl, 1% Triton X-100, 5% glycerol), and sonicated. Cell debris was removed by

centrifugation. The supernatant was collected and applied to ultracentrifugation at 150,000 *g* for 30 min, followed by purification of expressed protein with Nickel affinity gel and washed by 50 mM sodium phosphate, pH 7.4, 150 mM NaCl. The protein was eluted from the affinity resin by 50 mM sodium phosphate, pH 7.4, 150 mM NaCl, 250 mM imidazole and concentrated to about 3 mg/ml before further purification by gel filtration (Superdex-200, GE Healthcare). The buffer for gel filtration contained 50 mM Tris-HCl, pH 7.4, 150 mM NaCl, 5% glycerol and 1 mM DTT.

***In vitro* AMPK phosphorylation assay**

Bacterially expressed and purified AMPK (800 ng) was incubated with active LKB1/MO25/STRAD complex (200 ng) at 32 °C for 15 min in a kinase buffer containing 5 mM ATP with or without 60 μM AMP and 1 μg of AXIN1. Phosphorylation of AMPK was determined by immunoblotting.

Immunoprecipitation (IP) and immunoblotting

IP of endogenous AMPKα was performed as described previously[19], and was also used for IP ACC1 and ACC2, although with some modifications. Briefly, cells of one 15-cm dish (grown to 80% confluence) or 50 mg liver (for each lane) were collected and lysed with 500 μl of ice-cold lysis buffer (20 mM Tris-HCl, pH 7.5, 1 mM EDTA, 1 mM EGTA, 1% Triton X-100, 1 mM β-glycerolphosphate, with protease inhibitor cocktail. Note, note that 150 mM NaCl was used for IP of ACC1 and ACC2, and 50

mM NaCl was used for IP of AMPKα. Lysates were incubated with respective antibodies for 4 hr (ACC1 and ACC2) or overnight (AMPKα). Protein aggregates were pre-cleared by centrifugation at 20,000*g* for 10 min, and protein A/G beads (1:100) were then added into the lysates and mixed for another 1 (for ACC1 and ACC2) to 3 hr (for AMPKα). The beads were washed with 100 times volume of lysis buffer for 3 times at 4 °C and then mixed with an equal volume of 2× SDS sample buffer for immunoblotting.

To analyze the levels of p-AMPKα and p-ACC in MEFs, cells grown to 70-80% confluence in a well of a 6-well dish were lysed with 250 μl of ice-cold lysis buffer. The lysates were then centrifuged at 20,000 *g* for 10 min at 4 °C and an equal amount of 2× SDS sample buffer was into each supernatant. The levels of p-AMPKα and p-ACC were then analyzed by immunoblotting. To analyze the levels of p-AMPKα and p-ACC in liver, the freshly excised liver tissues were added with ice cold lysis buffer (10 μl/mg liver weight), followed by homogenization and centrifugation as described above. The lysates were then mixed with 2× SDS sample buffer and then subjected to immunoblotting. Levels of total proteins and the levels of phosphorylation of proteins were analyzed on separate gels and representative images were shown. The band intensities on developed films were quantified using Image J software (National Institutes of Health Freeware).

Fluorescence microscopy

HEK293T infected with different fusion constructs of β1 were grown on glass

683 coverslips in 6-well dishes and were cultured to 60-80% confluence. Cells were fixed
684 with 1 ml of 4% formaldehyde (diluted in PBS) at room temperature for 20 min. They
685 were rinsed twice with 1 ml PBS (room temperature) and then permeabilized with 1
686 ml of 0.1% Triton X-100 (diluted in PBS) for 5 min at 4 °C. Cells were rinsed twice
687 with 1 ml PBS, and were incubated with primary antibodies overnight at 4 °C. The
688 cells were then rinsed three times with 1 ml PBS, and then incubated with
689 Alexa-Fluor 594-conjugated anti mouse secondary antibody (Molecular Probes, cat.
690 A11032; diluted 1:100 in PBS) and Alexa-Fluor 488-conjugated anti-rabbit secondary
691 antibody (Molecular Probes, R37117; diluted 1:100 in PBS) for 8 hr at room
692 temperature in the dark. They were washed four times with 1 ml PBS, and then
693 mounted on glass slides using ProLong Diamond Antifade Mountant (Molecular
694 Probes, cat. P36970). Cells were imaged under a Zeiss LSM 780. Samples were
695 excited with an Ar gas laser (Zeiss, laser module LGK 7812) using a 488-nm laser
696 line for Alexa-Fluor 488 dye (green channel), and with a HeNe gas laser (Zeiss, LGK
697 7512 PF) using a 594-nm laser line for Alexa-Fluor 594 dye (red channel). Confocal
698 microscope images were taken with a 63× oil objective and representative images
699 were shown. The parameters, including 'PMT voltage', 'Offset', 'Pinhole' and 'Gain',
700 were kept unchanged between each image taken.
701
702 **CE-MS-based analysis of AMP, ADP, and ATP**
703 Sample preparation for CE (capillary electrophoresis)-MS was carried out as
704 described previously[75, 76], with some modifications. In general, each measurement

required cells collected from a 10-cm dish (60-70% confluence) or 100 mg of liver tissue. For analysis of metabolites, cells were rinsed with 20 ml of 5% mannitol solution (dissolved in water) and instantly frozen in liquid nitrogen. Cells were then lysed with 1 ml of methanol containing internal standards 1 [IS1 (Human Metabolome Technologies, H3304-1002, 1:200), used to standardize the metabolite intensity and to adjust the migration time], and were scrapped off from the dish. For analysis of metabolites in liver, the fleshly excised tissue was freeze-clamped first, then washed in pre-cooled 5% mannitol solution and grinded in 1 ml of methanol with 50 μM IS1. The lysate was then mixed with 1 ml of chloroform and 400 μl of water by 20 s of vortexing. After centrifugation at 15,000*g* for 15 min at 4 °C, 450 μl of aqueous phase was collected and was then filtrated through a 5 kDa cutoff filter (Millipore, cat. UFC3LCCNB-HMT) by centrifuging at 10,000*g* for 3 hr at 4 °C. Simultaneously, the quality control (QC) sample was prepared by combining 100 μl of the aqueous phase from each samples and then filtered. The filtered aqueous phase was then freeze-dried in a vacuum concentrator and then dissolved in water containing internal standards 3 [IS3 (Human Metabolome Technologies, H3304-1104, 1:200), to adjust the migration time]. 20 μl of re-dissolved solution was then loaded into an injection vial with a conical insert for CE-TOF MS (Agilent Technologies 7100, equipped with 6224 mass spectrometer) analysis. For quantification of AMP and ATP, [U-^{13}C, ^{15}N]AMP and [U-^{13}C, ^{15}N]ATP were used to generate standard curves by plotting the ratios of detected labelled AMP or ATP (areas) to the products of IS1 and IS3, against the added concentrations of labelled AMP or ATP. The standard curve of [U-^{13}C,

^{15}N]AMP was also used for quantification of ZMP, because of the structural similarity between them. The amount of AMP, ZMP, and ATP were then estimated according to equations generated from standard curves. The average cell volume, 2263 μm^3, was determined by Imaris 7.4.0 software (Bitplane) from the axial image stacks of CDFA-SE labelled MEFs taken under Zeiss LSM780.

HPLC-MS-based analysis of short-chain acyl-CoA

Procedure of preparing samples for HPLC-MS-based acyl-CoA analysis was identical to that described in the CE-MS section, except that cells or liver tissues were rinsed in PBS, and that ^{13}C2:0-CoA (150 μg/l) and ^{13}C3:0-CoA (200 μg/l) prepared in methanol were added as internal standards. Some 800 μl of the aqueous phase of each sample was collected after centrifugation at 15,000 *g* for 15 min at 4 °C and was lyophilized in a vacuum concentrator. Samples were then re-dissolved in 20 μl of ice-cold 20% methanol. Measurement of acetyl- and malonyl-CoAs was based on a previous study[77] using a QTRAP (SCIEX, QTRAP 6500 plus) mass spectrometer interfaced with a UPLC system (Waters, ACQUITY UPLC system). Some 5 μl of each sample were injected onto an Acquity HSS T3 column (2.1 × 50 mm, 1.7 μm, Waters) attached to an Acquity BEH C18 pre-column (2.1 × 5 mm, 1,7 μm, Waters). Mobile phases A and B were water and acetonitrile, respectively (both contains 10 mM ammonium acetate and 0.05% ammonium hydroxide). The column temperature was maintained at 30 °C and autosampler temperature at 8 °C. The gradients were as follows: t = 0 min, 3% B; t = 1 min, 3% B; t = 13 min, 15% B; t = 14.1 min, 100% B; t = 14.7 min, 100% B; t =

14.71 min, 3% B; t = 17 min, 3% B. Mass spectrometer was run in positive mode with multiple reactions monitoring mode (MRM), and declustering potentials (DP) and collision energies (CE) were set at 200 V and 38 V, respectively (optimized using ^{13}C2:0- and ^{13}C3:0-CoA). The following transitions and retention time were used for monitoring each compound: 812.0, 305.3, and 2.2 min for ^{13}C2:0-CoA, 810.1, 303.1, and 2.2 min for acetyl-CoA, 856.9, 350.2, and 0.8 min for ^{13}C3:0-CoA, and 854.1, 347.1, and 0.8 min for malonyl-CoA. It should be noted that acyl-CoAs were extremely easy to degrade even frozen at -80 °C, so no pause was taken during the whole analytic process and no more than 6 samples were re-dissolved and kept in autosampler at one time.

Statistical analysis

1-way or 2-way ANOVA with post hoc analysis was used to compare values among different experimental groups. For experiments with only two groups, a two-tailed Student's *t* test was used as specified in the figure legends. For ANOVA, the homogeneity of variance was firstly tested by Levene's test. If the results are similar, the Tukey's test was preceded, and if not, the Games-Howell's test was processed. Similar procedures were followed when Student's t test was performed. No samples or animals were excluded from the analysis. Tests were performed with SPSS Statistics 17.0 program, and $p < 0.05$ was considered statistically significant. Statistical significance is shown as * $p < 0.05$, ** $p < 0.01$, *** $p < 0.001$; N.S., not significant.

ACKNOWLEDGMENTS

ACC1-floxed mouse (Stock No. 030954, The Jackson Laboratory) was a generous gift from Prof. Jay Horton (UT Southwestern Medical Center), and the *ACC2*$^{-/-}$ mouse from Prof. Tian Xu (Institute of Developmental Biology and Molecular Medicine, Fudan University). Heterotrimeric AMPK cloned into pET21b was a generous gift from Prof. Dietbert Neumann (Swiss Federal Institute of Technology). We also thank Jiayuan Zhang from Xiamen University for the artwork of Fig. 4e. This work was supported by grants from the National Key R&D Program of China (2016YFA0502001) and the National Natural Science Foundation of China (#31730058, #31430094, #31601152 and #31690101) through S.-C.L., by the Open Research Fund of State Key Laboratory of Cellular Stress Biology, Xiamen University (SKLCSB2017KF002) through H.-L.P., and by Wellcome Trust (204766/Z/16/Z) through D.G.H.

AUTHOR CONTRIBUTIONS

Y.Z., C.-S.Z., M.L. and S.-C.L. conceived the study and designed the experiments. Y.Z., C.-S.Z. and M.L. performed the subcellular fractionation, immunoprecipitation, *in vitro* reconstitution and the associated western blot analyses with assistance from S.A.H, T.M., J.-W.F., X.T., Q.Q. and Y.-Q.W. Y.Z., W.W., Z.W. and C.Z. performed the CE-MS- and HPLC-MS-based analysis of adenylates and CoAs under the guidance of H.-L.P. M.L. performed the confocal imaging acquisition. Z.Y., S.-Y.L., H.-L.P. and D.G.H. helped with discussion and interpretation of results. D.G.H. and

S.-C.L. wrote the manuscript.

ADDITIONAL INFORMATION

Supplementary Information accompanies this paper at https://doi.org/10.1038/.

Competing interests: The authors declare no competing interests.

REFERENCES

1 Carling D, Thornton C, Woods A, Sanders MJ. AMP-activated protein kinase: new regulation, new roles? *The Biochemical journal* 2012; **445**:11-27.

2 Steinberg GR, Kemp BE. AMPK in Health and Disease. *Physiological reviews* 2009; **89**:1025-1078.

3 Herzig S, Shaw RJ. AMPK: guardian of metabolism and mitochondrial homeostasis. *Nature reviews Molecular cell biology* 2017.

4 Lin SC, Hardie DG. AMPK: sensing glucose as well as cellular energy status. *Cell Metab* 2017; **27**:299-313.

5 Viollet B, Horman S, Leclerc J *et al.* AMPK inhibition in health and disease. *Critical reviews in biochemistry and molecular biology* 2010; **45**:276-295.

6 Scott JW, Hawley SA, Green KA *et al.* CBS domains form energy-sensing modules whose binding of adenosine ligands is disrupted by disease mutations. *J Clin Invest* 2004; **113**:274-284.

7 Xiao B, Heath R, Saiu P *et al.* Structural basis for AMP binding to mammalian AMP-activated protein kinase. *Nature* 2007; **449**:496-500.

8 Gu X, Yan Y, Novick SJ *et al.* Deconvoluting AMP-dependent kinase (AMPK) adenine nucleotide binding and sensing. *J Biol Chem* 2017; **292**:12653-12666.

9 Ross FA, Jensen TE, Hardie DG. Differential regulation by AMP and ADP of AMPK complexes containing different gamma subunit isoforms. *Biochem J* 2016; **473**:189-199.

10 Hawley SA, Pan DA, Mustard KJ *et al.* Calmodulin-dependent protein kinase kinase-beta is an alternative upstream kinase for AMP-activated protein kinase. *Cell Metab* 2005; **2**:9-19.

11 Woods A, Dickerson K, Heath R *et al.* Ca2+/calmodulin-dependent protein kinase kinase-beta acts upstream of AMP-activated protein kinase in mammalian cells. *Cell Metab* 2005; **2**:21-33.

12 Hurley RL, Anderson KA, Franzone JM, Kemp BE, Means AR, Witters LA. The Ca^{2+}/calmoldulin-dependent protein kinase kinases are AMP-activated protein kinase kinases. *J Biol Chem* 2005; **280**:29060-29066.

13 Salt IP, Johnson G, Ashcroft SJH, Hardie DG. AMP-activated protein kinase is activated by low glucose in cell lines derived from pancreatic b cells, and may regulate insulin release. *Biochem J* 1998; **335**:533-539.

14 Zhang CS, Hawley SA, Zong Y *et al.* Fructose-1,6-bisphosphate and aldolase mediate glucose sensing by AMPK. *Nature* 2017; **548**:112-116.

15 Gonzalez PS, O'Prey J, Cardaci S *et al.* Mannose impairs tumour growth and enhances chemotherapy. *Nature* 2018; **563**:719-723.

16 Nada S, Hondo A, Kasai A *et al.* The novel lipid raft adaptor p18 controls endosome dynamics by anchoring the MEK-ERK pathway to late endosomes. *Embo J* 2009; **28**:477-489.

17 Bar-Peled L, Schweitzer LD, Zoncu R, Sabatini DM. Ragulator is a GEF for the rag GTPases that signal amino acid levels to mTORC1. *Cell* 2012; **150**:1196-1208.

18 Zhang CS, Jiang B, Li M *et al.* The lysosomal v-ATPase-Ragulator complex Is a common activator for AMPK and mTORC1, acting as a switch between catabolism and anabolism. *Cell Metab* 2014; **20**:526-540.

19 Zhang YL, Guo H, Zhang CS *et al.* AMP as a low-energy charge signal autonomously initiates assembly of AXIN-AMPK-LKB1 complex for AMPK

activation. *Cell Metab* 2013; **18**:546-555.

20 Miyamoto T, Rho E, Sample V *et al.* Compartmentalized AMPK signaling illuminated by genetically encoded molecular sensors and actuators. *Cell reports* 2015; **11**:657-670.

21 Salt IP, Celler JW, Hawley SA *et al.* AMP-activated protein kinase - greater AMP dependence, and preferential nuclear localization, of complexes containing the a2 isoform. *Biochem J* 1998; **334**:177-187.

22 Kazgan N, Williams T, Forsberg LJ, Brenman JE. Identification of a nuclear export signal in the catalytic subunit of AMP-activated protein kinase. *Mol Biol Cell* 2010; **21**:3433-3442.

23 Vincent O, Townley R, Kuchin S, Carlson M. Subcellular localization of the Snf1 kinase is regulated by specific beta subunits and a novel glucose signaling mechanism. *Genes Dev* 2001; **15**:1104-1114.

24 Liang J, Xu ZX, Ding Z *et al.* Myristoylation confers noncanonical AMPK functions in autophagy selectivity and mitochondrial surveillance. *Nature communications* 2015; **6**:7926.

25 Yi C, Tong J, Lu P *et al.* Formation of a Snf1-Mec1-Atg1 Module on Mitochondria Governs Energy Deprivation-Induced Autophagy by Regulating Mitochondrial Respiration. *Developmental cell* 2017; **41**:59-71 e54.

26 Tsou P, Zheng B, Hsu CH, Sasaki AT, Cantley LC. A fluorescent reporter of AMPK activity and cellular energy stress. *Cell metabolism* 2011; **13**:476-486.

27 Warden SM, Richardson C, O'Donnell J, Jr., Stapleton D, Kemp BE, Witters LA. Post-translational modifications of the beta-1 subunit of AMP-activated protein kinase affect enzyme activity and cellular localization. *Biochem J* 2001; **354**:275-283.

28 Oakhill JS, Chen ZP, Scott JW *et al.* beta-Subunit myristoylation is the gatekeeper for initiating metabolic stress sensing by AMP-activated protein kinase (AMPK). *Proc Natl Acad Sci USA* 2010; **107**:19237-19241.

29 Davies SP, Sim AT, Hardie DG. Location and function of three sites phosphorylated on rat acetyl-CoA carboxylase by the AMP-activated protein kinase.

876 *Eur J Biochem* 1990; **187**:183-190.

877 30 Winder WW, Wilson HA, Hardie DG *et al.* Phosphorylation of rat muscle
878 acetyl-CoA carboxylase by AMP-activated protein kinase and protein kinase A. *J*
879 *Appl Physiol* 1997; **82**:219-225.

880 31 Abu-Elheiga L, Brinkley WR, Zhong L, Chirala SS, Woldegiorgis G, Wakil SJ.
881 The subcellular localization of acetyl-CoA carboxylase 2. *Proc Natl Acad Sci U S A*
882 2000; **97**:1444-1449.

883 32 Abu-Elheiga L, Oh W, Kordari P, Wakil SJ. Acetyl-CoA carboxylase 2 mutant
884 mice are protected against obesity and diabetes induced by high-fat/high-carbohydrate
885 diets. *Proc Natl Acad Sci USA* 2003; **100**:10207-10212.

886 33 Wakil SJ, Abu-Elheiga LA. Fatty acid metabolism: target for metabolic syndrome.
887 *Journal of lipid research* 2009; **50 Suppl**:S138-143.

888 34 Hardie DG, Ross FA, Hawley SA. AMPK: a nutrient and energy sensor that
889 maintains energy homeostasis. *Nature Rev Mol Cell Biol* 2012; **13**:251-262.

890 35 Li Y, Xu S, Mihaylova MM *et al.* AMPK phosphorylates and Inhibits SREBP
891 activity to attenuate hepatic steatosis and atherosclerosis in diet-induced
892 insulin-resistant mice. *Cell Metab* 2011; **13**:376-388.

893 36 Qian X, Li X, Tan L *et al.* Conversion of PRPS hexamer to monomer by
894 AMPK-mediated phosphorylation inhibits nucleotide synthesis in response to energy
895 stress. *Cancer Discov* 2018; **8**:94-107.

896 37 Inoki K, Zhu T, Guan KL. TSC2 mediates cellular energy response to control cell
897 growth and survival. *Cell* 2003; **115**:577-590.

898 38 Gwinn DM, Shackelford DB, Egan DF *et al.* AMPK phosphorylation of raptor
899 mediates a metabolic checkpoint. *Mol Cell* 2008; **30**:214-226.

900 39 Zoncu R, Bar-Peled L, Efeyan A, Wang S, Sancak Y, Sabatini DM. mTORC1
901 senses lysosomal amino acids through an inside-out mechanism that requires the
902 vacuolar H(+)-ATPase. *Science* 2011; **334**:678-683.

40 Efeyan A, Zoncu R, Chang S *et al.* Regulation of mTORC1 by the Rag GTPases is necessary for neonatal autophagy and survival. *Nature* 2013; **493**:679-683.

41 Pehmoller C, Treebak JT, Birk JB *et al.* Genetic disruption of AMPK signaling abolishes both contraction- and insulin-stimulated TBC1D1 phosphorylation and 14-3-3 binding in mouse skeletal muscle. *Am J Physiol Endocrinol Metab* 2009; **297**:E665-E675.

42 Vichaiwong K, Purohit S, An D *et al.* Contraction regulates site-specific phosphorylation of TBC1D1 in skeletal muscle. *The Biochemical journal* 2010; **431**:311-320.

43 Egan DF, Shackelford DB, Mihaylova MM *et al.* Phosphorylation of ULK1 (hATG1) by AMP-activated protein kinase connects energy sensing to mitophagy. *Science* 2011; **331**:456-461.

44 Kim J, Kundu M, Viollet B, Guan KL. AMPK and mTOR regulate autophagy through direct phosphorylation of Ulk1. *Nature cell biology* 2011; **13**:132-141.

45 Kim J, Kim YC, Fang C *et al.* Differential regulation of distinct Vps34 complexes by AMPK in nutrient stress and autophagy. *Cell* 2013; **152**:290-303.

46 Youle RJ, van der Bliek AM. Mitochondrial fission, fusion, and stress. *Science* 2012; **337**:1062-1065.

47 Toyama EQ, Herzig S, Courchet J *et al.* Metabolism. AMP-activated protein kinase mediates mitochondrial fission in response to energy stress. *Science* 2016; **351**:275-281.

48 Kim N, Lee JO, Lee HJ *et al.* AMPKalpha2 translocates into the nucleus and interacts with hnRNP H: implications in metformin-mediated glucose uptake. *Cellular signalling* 2014; **26**:1800-1806.

49 Wu D, Hu D, Chen H *et al.* Glucose-regulated phosphorylation of TET2 by AMPK reveals a pathway linking diabetes to cancer. *Nature* 2018; **559**:637-641.

50 Chia IV, Costantini F. Mouse axin and axin2/conductin proteins are functionally equivalent in vivo. *Molecular and cellular biology* 2005; **25**:4371-4376.

931 51 Nusse R, Clevers H. Wnt/beta-Catenin Signaling, Disease, and Emerging
932 Therapeutic Modalities. *Cell* 2017; **169**:985-999.

933 52 Corton JM, Gillespie JG, Hawley SA, Hardie DG.
934 5-aminoimidazole-4-carboxamide ribonucleoside. A specific method for activating
935 AMP-activated protein kinase in intact cells? *Eur J Biochem* 1995; **229**:558-565.

936 53 Faupel RP, Seitz HJ, Tarnowski W, Thiemann V, Weiss C. The problem of tissue
937 sampling from experimental animals with respect to freezing technique, anoxia, stress
938 and narcosis. A new method for sampling rat liver tissue and the physiological values
939 of glycolytic intermediates and related compounds. *Archives of biochemistry and*
940 *biophysics* 1972; **148**:509-522.

941 54 Dale S, Wilson WA, Edelman AM, Hardie DG. Similar substrate recognition
942 motifs for mammalian AMP-activated protein kinase, higher plant HMG-CoA
943 reductase kinase-A, yeast SNF1, and mammalian calmodulin-dependent protein
944 kinase I. *FEBS letters* 1995; **361**:191-195.

945 55 Scott JW, van Denderen BJ, Jorgensen SB *et al.* Thienopyridone drugs are
946 selective activators of AMP-activated protein kinase beta1-containing complexes.
947 *Chem Biol* 2008; **15**:1220-1230.

948 56 Luo W, Zou H, Jin L *et al.* Axin contains three separable domains that confer
949 intramolecular, homodimeric, and heterodimeric interactions involved in distinct
950 functions. *The Journal of biological chemistry* 2005; **280**:5054-5060.

951 57 Kim SE, Huang H, Zhao M *et al.* Wnt stabilization of beta-catenin reveals
952 principles for morphogen receptor-scaffold assemblies. *Science* 2013; **340**:867-870.

953 58 Xin FJ, Wang J, Zhao RQ, Wang ZX, Wu JW. Coordinated regulation of AMPK
954 activity by multiple elements in the alpha-subunit. *Cell research* 2013; **23**:1237-1240.

955 59 Li X, Wang L, Zhou XE *et al.* Structural basis of AMPK regulation by adenine
956 nucleotides and glycogen. *Cell research* 2015; **25**:50-66.

957 60 Ross FA, MacKintosh C, Hardie DG. AMP-activated protein kinase: a cellular
958 energy sensor that comes in 12 flavours. *FEBS J* 2016; **283**:2987-3001.

959 61 Olivier S, Foretz M, Viollet B. Promise and challenges for direct small molecule

960 AMPK activators. *Biochemical pharmacology* 2018; **153**:147-158.

961 62 Khan AS, Frigo DE. A spatiotemporal hypothesis for the regulation, role, and
962 targeting of AMPK in prostate cancer. *Nature reviews Urology* 2017; **14**:164-180.

963 63 Boudaba N, Marion A, Huet C, Pierre R, Viollet B, Foretz M. AMPK
964 Re-Activation Suppresses Hepatic Steatosis but its Downregulation Does Not
965 Promote Fatty Liver Development. *EBioMedicine* 2018; **28**:194-209.

966 64 Cao Y, Bojjireddy N, Kim M *et al.* Activation of gamma2-AMPK Suppresses
967 Ribosome Biogenesis and Protects Against Myocardial Ischemia/Reperfusion Injury.
968 *Circulation research* 2017; **121**:1182-1191.

969 65 Woods A, Williams JR, Muckett PJ *et al.* Liver-Specific Activation of AMPK
970 Prevents Steatosis on a High-Fructose Diet. *Cell reports* 2017; **18**:3043-3051.

971 66 Su H, Yang F, Wang Q *et al.* VPS34 Acetylation Controls Its Lipid Kinase
972 Activity and the Initiation of Canonical and Non-canonical Autophagy. *Molecular*
973 *cell* 2017; **67**:907-921 e907.

974 67 Cheong H, Lindsten T, Wu J, Lu C, Thompson CB. Ammonia-induced autophagy
975 is independent of ULK1/ULK2 kinases. *Proceedings of the National Academy of*
976 *Sciences of the United States of America* 2011; **108**:11121-11126.

977 68 Soeters MR, Soeters PB, Schooneman MG, Houten SM, Romijn JA. Adaptive
978 reciprocity of lipid and glucose metabolism in human short-term starvation. *American*
979 *journal of physiology Endocrinology and metabolism* 2012; **303**:E1397-1407.

980 69 Cahill GF, Jr. Starvation in man. *Clinics in endocrinology and metabolism* 1976;
981 **5**:397-415.

982 70 Pilegaard H, Saltin B, Neufer PD. Effect of short-term fasting and refeeding on
983 transcriptional regulation of metabolic genes in human skeletal muscle. *Diabetes* 2003;
984 **52**:657-662.

985 71 Li TY, Sun Y, Liang Y *et al.* ULK1/2 Constitute a Bifurcate Node Controlling
986 Glucose Metabolic Fluxes in Addition to Autophagy. *Molecular cell* 2016;
987 **62**:359-370.

988 72 Abe Y, Hines IN, Zibari G *et al.* Mouse model of liver ischemia and reperfusion
989 injury: method for studying reactive oxygen and nitrogen metabolites in vivo. *Free*
990 *radical biology & medicine* 2009; **46**:1-7.

991 73 Wieckowski MR, Giorgi C, Lebiedzinska M, Duszynski J, Pinton P. Isolation of
992 mitochondria-associated membranes and mitochondria from animal tissues and cells.
993 *Nature protocols* 2009; **4**:1582-1590.

994 74 Kobayashi T, Beuchat MH, Chevallier J *et al.* Separation and characterization of
995 late endosomal membrane domains. *The Journal of biological chemistry* 2002;
996 **277**:32157-32164.

997 75 Zhao J, Hu C, Zeng J *et al.* Study of polar metabolites in tobacco from different
998 geographical origins by using capillary electrophoresis–mass spectrometry.
999 *Metabolomics* 2014; **10**:805-815.

1000 76 Zhao Y, Zhao J, Zhao C *et al.* A metabolomics study delineating geographical
1001 location-associated primary metabolic changes in the leaves of growing tobacco
1002 plants by GC-MS and CE-MS. *Scientific reports* 2015; **5**:16346.

1003 77 Wang S, Wang Z, Zhou L, Shi X, Xu G. Comprehensive Analysis of Short-,
1004 Medium-, and Long-Chain Acyl-Coenzyme A by Online Two-Dimensional Liquid
1005 Chromatography/Mass Spectrometry. *Analytical chemistry* 2017; **89**:12902-12908.

1006

Figure Legends

Fig. 1 Basal AMP Is Sufficient for Activation of the Lysosomal Pool of AMPK. **a** Low glucose exclusively activates the lysosomal pool of AMPK in MEFs. MEFs were grown in full medium and then switched to DMEM containing reduced concentrations of glucose for 2 hr, or to DMEM lacking both glucose and glutamine (starvation for glucose plus glutamine, GS+QS). Cytosolic, lysosomal, and mitochondrial fractions were prepared following the methods described in "Materials and Methods". Fractions were then subjected to analysis of p-AMPKα and p-ACC by immunoblotting using the indicated antibodies, followed by densitometry analysis. Statistical analysis results were shown in mean ± SD; *** $p < 0.001$, * $p < 0.05$, N.S., not significant by ANOVA, n = 3. **b** AMP:ATP and ADP:ATP ratios are not changed in MEFs in low glucose. Adenylate nucleotide ratios in MEFs treated as in (**a**) were measured by CE-MS. Results are mean ± SD; N.S., not significant by ANOVA, n = 3. **c** Starvation-induced AMPK activation in liver takes place on lysosome. Mice were fed ad libitum or starved for 16 hr, followed by fractionation of cytosol, lysosomes and mitochondria from liver homogenates, and subsequent immunoblotting using the indicated antibodies. **d** AMP/ATP and ADP/ATP ratios are unchanged in the liver of starved mice. Mice were fed or starved as in (**c**), freeze-clamped liver samples prepared, and AMP/ATP and ADP/ATP ratios measured by CE–MS. Results are mean ± SD, n = 6; N.S., not significant by Student's t-test. **e, f** ACC1, but not ACC2, is phosphorylated in MEFs starved for glucose or in the liver of starved mice. MEFs

were glucose starved or severely starved as in (**a**), while mice were fed or starved as in (**c**). Endogenous ACC1 and ACC2 in MEFs (**e**) or mice livers (**f**) were individually immunoprecipitated, followed by immunoblotting. Statistical analysis data of experiments in (**e**) were shown in mean ± SD; *** $p < 0.001$, N.S., not significant by ANOVA, n = 3. **g** Phosphorylation of SREBP1c, TSC2, Raptor, HDAC4, ULK1, Beclin-1 and TBC1D1, but not MFF, is observed in low glucose. HEK293T cells or MEFs were incubated in DMEM medium with (25 mM) or without glucose for 2 hr, followed by analysis of phosphorylation levels of AMPK substrates as indicated. Statistical analysis data were shown in mean ± SD; * $p < 0.05$, ** $p < 0.01$, *** $p < 0.001$, by ANOVA, n = 3. **h** AXIN1 and AXIN2 are functionally equivalent in the lysosomal pathway of AMPK activation in HEK293T cells. *AXIN2*$^{-/-}$ HEK293T cells and its wildtype control were infected with lentivirus expressing siRNA against *AXIN1*. Cells were starved for glucose for 2 hr and then lyzed, followed by immunoblotting. **i** Re-introduction of AXIN2 into *AXIN1*$^{-/-}$ MEFs restores glucose starvation-induced AMPK activation. *AXIN1*$^{-/-}$ MEFs (and its wildtype control) were infected with lentivirus expressing HA-tagged AXIN2. Cells were then starved for glucose for 2 hr, followed by immunoblotting. Experiments in this figure were performed three times, except (**d)** and (**i)** twice. See also Supplementary information, Fig. S1

Fig. 2 Modest Increases in AMP Activate Cytosolic AMPK in an AXIN1-dependent Manner. **a** Glucose starvation activates both lysosomal and cytosolic AMPK in a

LAMTOR1-independent manner in HEK293 cells. HEK293 cells were infected with siRNA against *LAMTOR1*, and were deprived of glucose or both glucose and glutamine for 2 hr, followed by fractionation and immunoblotting. Statistical analysis data were shown on lower panel, in mean ± SD; N.S., not significant by ANOVA, n = 3. **b** AXIN is required for glucose starvation-induced, cytosolic AMPK activation in HEK293 cells. Cells were infected with siRNA against *AXIN1*, followed by glucose starvation or severe nutrient starvation as in (**a**). P-AMPKα level was then determined by immunoblotting, followed by densitometry analysis, and the data were shown in mean ± SD; *** $p < 0.001$, * $p < 0.05$ by ANOVA, n = 3. **c** The AMP levels and AMP/ATP and ADP/ATP ratios are modestly increased in HEK293 cells, unlike MEFs, after glucose starvation. HEK293 cells were regularly cultured (Nor), starved for glucose for 2 hr (GS), or starved for both glucose and glutamine for 2 hr (GS+QS), followed by determination of concentrations (upper panel) and ratios (lower panel) of adenylate nucleotide by CE-MS. Results are mean ± SD; ** $p < 0.01$, *** $p < 0.001$ by ANOVA, n = 3. **d** ACC1, but not ACC2, is phosphorylated in HEK293 cells after glucose starvation. Cells were starved as in (**b**), in which endogenous ACC1 and ACC2 were individually immunoprecipitated and analyzed by immunoblotting. Statistical analysis data were shown in mean ± SD; *** $p < 0.001$ by ANOVA, n = 3. **e** AICAR at low concentrations activates cytosolic AMPK as does moderately increased AMP. MEFs were treated with 0.6 mM AICAR for 2 hr, or starved for glucose or both glucose and glutamine for 2 hr, followed by fractionation and immunoblotting. **f** ACC1, but not ACC2, is phosphorylated in MEFs treated with low

concentrations of AICAR. MEFs were treated with AICAR or severely starved as in (**e**). The endogenous ACC1 and ACC2 were then individually immunoprecipitated and analyzed by immunoblotting. **g, h** AICAR at low concentrations activates cytosolic AMPK in an AXIN1-dependent, LAMTOR1-independent manner. *AXIN1*$^{-/-}$ MEFs (**g**) and *LAMTOR1*$^{-/-}$ MEFs (**h**) were treated with AICAR or severely starved as in (**e**), followed by fractionation and immunoblotting. **i** Knockout of *AXIN1* blocked the association between LKB1 and AMPK under moderate AMP in MEFs. Cells were treated with 0.6 mM AICAR for 2 hr, followed by fractionation. Endogenous AMPKα from lysosomal and cytosolic fractions was then immunoprecipitated, and its interaction with AXIN1 and LKB1 was analyzed by immunoblotting with indicated antibodies. Experiments in (**a**), (**b**), (**d**), (**g**), (**h**) and (**i**) were performed three times, and the others twice. See also Supplementary information, Fig. S2

Fig. 3 The Mitochondria-localized ACC2 Is Phosphorylated by AMPK Only after Severe Nutrient Stress. **a** Severe nutrient stress causes a full activation of AMPK in the cytosolic, lysosomal and mitochondrial pools. MEFs were starved for both glucose and glutamine for 2 hr, treated with 2 mM AICAR for 2 hr, or starved for glucose for 2 hr as a control, followed by fractionation and immunoblotting for p-AMPKα. Statistical analysis data were shown in mean ± SD; ** $p < 0.01$, N.S., not significant by ANOVA, n = 3. **b** The AMP levels, and ratios of AMP/ATP and ADP/ATP in MEFs under severe nutrient stress. Cells were treated with 2 mM AICAR or starved for glucose as in (**a**), in which adenylate concentrations (upper

1095 panel) and nucleotide ratios (lower panel) were measured by CE-MS. Note that in the
1096 group of AICAR treatment, the total levels of AMP were composed of the amount of
1097 ZMP-converted AMP (estimated according to a previous study[52]) and that of
1098 endogenous AMP. Results are mean ± SD; *** $p < 0.001$ by ANOVA, n = 3. **c** Both
1099 ACC1 and ACC2 are phosphorylated in MEFs under severe nutrient stress. Cells were
1100 treated as in (**a**). The endogenous ACC1 and ACC2 were then individually
1101 immunoprecipitated and analyzed by immunoblotting. Statistical analysis data were
1102 shown in mean ± SD; *** $p < 0.001$, N.S., not significant by ANOVA, n = 3. **d**
1103 ACC1/2 in both cytosolic and mitochondrial pools can be phosphorylated in MEFs
1104 under severe nutrient stress. Cells were treated with AICAR or starved for glucose as
1105 in (**a**), followed by fractionation and immunoblotting for p-ACC. Statistical analysis
1106 data were shown in mean ± SD; *** $p < 0.001$, ** $p < 0.01$, N.S., not significant by
1107 ANOVA, n = 3. **e** ACC2 can only be phosphorylated in MEFs under severe nutrient
1108 stress. *ACC1*$^{-/-}$ and *ACC2*$^{-/-}$ MEFs were starved for glucose for 2 hr, treated with 0.6
1109 mM AICAR for 2 hr, or starved for both glucose and glutamine for 2 hr, followed by
1110 immunoblotting. **f** Levels of acetyl-coA and malonyl-CoA, the substrate and product
1111 respectively of ACC, in MEFs under different kinds of stress. Cells were starved or
1112 treated with AICAR as in (**a**), except that 20 μM TOFA (2-hr-treatment) was used as
1113 an additional control, followed by determining acetyl-coA and malonyl-CoA levels by
1114 HPLC-MS. Results are mean ± SD; *** $p < 0.001$, N.S., not significant by ANOVA,
1115 n = 3. **g** All pools of AMPK, in the cytosol, lysosome and mitochondria can be
1116 activated in liver of mice subjected to hepatic ischemia. Mice were anesthetized. The

1117 left lateral and median lobes of liver were deprived of blood flow for 10 min by
1118 cross-clamping the hepatic artery and portal vein (described in EXPERIMENTAL
1119 PROCEDURES). Liver homogenates were then subjected to fractionation as in Fig.
1120 1c, followed by immunoblotting. **h, i** AMP/ATP and ADP/ATP ratios, acetyl-coA and
1121 malonyl-coA levels in livers from mice under starvation or hepatic ischemia. Mice
1122 were starved for 16 hr or subjected to hepatic ischemia (for 10 min), followed by
1123 measurement of AMP/ATP and ADP/ATP ratios by CE-MS (**h**) or acetyl-coA and
1124 malonyl-coA levels by HPLC-MS (**i**). Results are mean ± SD; *** $p < 0.001$ by
1125 Student's t-test (**h**), ** $p < 0.01$, N.S., not significant by ANOVA (**i**), $n = 6$. **j** A
1126 schematic diagram showing the three fusion constructs of the β1 subunit (with
1127 modifications at the N-terminus) that allow AMPK to locate on lysosomal surface,
1128 mitochondrial outer membrane, or in cytosol. **k** ACC2 can only be phosphorylated by
1129 cytosol-localized and the mitochondrion-localized AMPK. AMPKβ-DKO HEK293T
1130 cells were infected with HA-tagged lyso-β1 (left panel), cyto-β1 (middle panel) and
1131 mito-β1 (right panel), respectively. Cells were then treated with 1 μM A-769662 for 2
1132 hr to allow full activation of AMPK, followed by fractionation and immunoblotting
1133 for analyzing p-AMPKα, or by immunoprecipitation and immunoblotting for
1134 analyzing p-ACC1 and p-ACC2. Experiments in (**a**), (**c**), (**d**), (**e**), (**g**) and (**k**) were
1135 performed three times, and the others twice. See also Supplementary information, Fig.
1136 S3, S4
1137
1138 **Fig. 4** Roles of AMP in the Hierarchical Activation of AMPK. **a** AMPKγ1-D317A

impairs glucose-starvation-induced AMPK activation. HA-tagged AMPK-γ1 and its D317A mutant were re-introduced into AMPKγ-TKO HEK293T cells. Cells were then deprived of glucose for 2 hr, followed by immunoblotting. **b, c** AMPKγ2-R531G blocks the phosphorylation of cytosolic and mitochondrial AMPK under moderate and high AMP levels. HA-tagged AMPK-γ2 and its R531G mutant were re-introduced into AMPKγ-TKO HEK293T cells. Cells were then deprived of glucose for 2 hr, followed by fractionation and immunoblotting for analyzing p-AMPKα (**b**), or by immunoprecipitation and immunoblotting for analyzing p-ACC1 and p-ACC2 (**c**). Statistical analysis data were shown in mean ± SD; *** $p < 0.001$, * $p < 0.05$, N.S., not significant by ANOVA, n = 3. **d** Knockout of *AK1* significantly dampens the activation of mitochondrial- and cytosolic-localized AMPK in high AMP conditions. MEFs with *AK1* being knocked out were deprived of glucose or both glucose and glutamine for 2 hr, followed by fractionation and immunoblotting for analyzing p-AMPKα. Statistical analysis data were shown in mean ± SD; *** $p < 0.001$, ** $p < 0.01$, * $p < 0.05$, N.S., not significant by ANOA, n = 3. **e** A simplified model depicting that the differentially compartmentalized pools of AMPK are activated with different dependencies on AXIN, and the severities of nutrient or energy stress. Glucose starvation, without increase of AMP levels, exclusively activates the lysosomal pool of AMPK through the AXIN-based pathway (❶) which phosphorylates substrates including ACC1, SREBP1, TSC2, Raptor, HDAC4, ULK1 and TBC1D1 to elicit early anti-anabolic roles. Moderately increased AMP levels, during the early phase of severe starvation or after treatment of low concentrations of

AICAR, activates cytosolic AMPK, in addition to the lysosomal AMPK (❷), still dependent on AXIN. When AMP levels go up further as a result of severe starvation, ischemia, or treatment of high concentrations of AICAR, cytosolic AMPK (❸) and mitochondrial AMPK (❹) are activated independently of AXIN, leading to phosphorylation of ACC2 and MFF and accelerating catabolic activities, along with all the other substrates that can be phsophorylated at lower AMP levels. Of note, TSC2 and Raptor can be phosphorylated by all the four modes to respectively inhibit mTORC1 activity. Experiments in this figure were performed three times. See also Supplementary information, Fig. S4

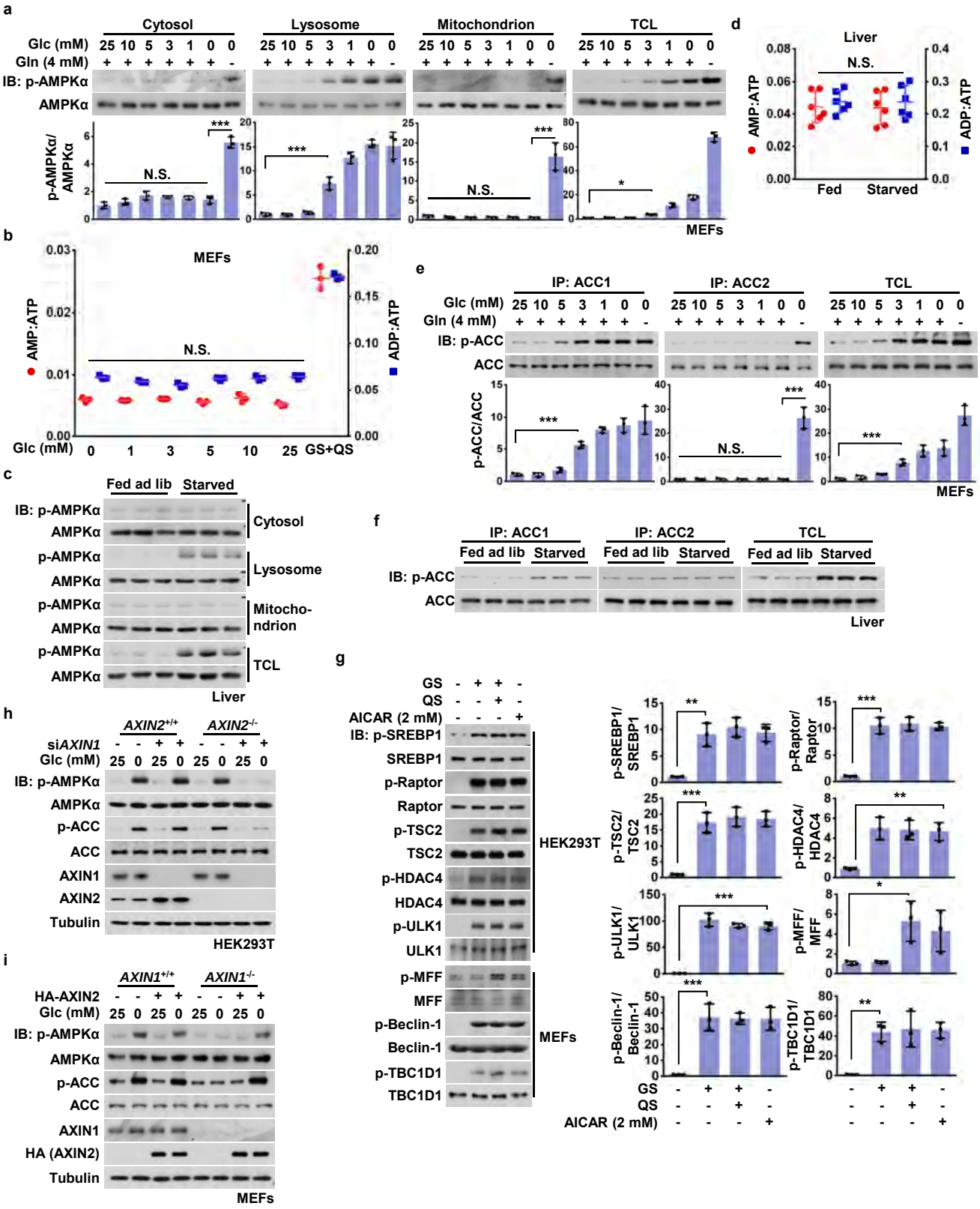
a
Cytosol
Lysosome
Mitochondrion
TCL
Glc (mM) 25 10 5 3 1 0 0
Gln (4 mM) + + + + + + -
IB: p-AMPKα
AMPKα
p-AMPKα/ AMPKα
N.S.
***
*
MEFs
b
MEFs
AMP:ATP
ADP:ATP
N.S.
Glc (mM) 0 1 3 5 10 25 GS+QS
c
Fed ad lib
Starved
IB: p-AMPKα
AMPKα
Cytosol
Lysosome
Mitocho-ndrion
TCL
Liver
d
Liver
N.S.
AMP:ATP
ADP:ATP
Fed
Starved
e
IP: ACC1
IP: ACC2
TCL
Glc (mM) 25 10 5 3 1 0 0
Gln (4 mM) + + + + + + -
IB: p-ACC
ACC
p-ACC/ACC
N.S.
MEFs
f
IP: ACC1
IP: ACC2
TCL
Fed ad lib
Starved
IB: p-ACC
ACC
Liver
g
GS - + + -
QS - - + -
AICAR (2 mM) - - - +
IB: p-SREBP1
SREBP1
p-Raptor
Raptor
p-TSC2
TSC2
p-HDAC4
HDAC4
p-ULK1
ULK1
HEK293T
p-MFF
MFF
p-Beclin-1
Beclin-1
p-TBC1D1
TBC1D1
MEFs
p-SREBP1/ SREBP1
p-Raptor/ Raptor
p-TSC2/ TSC2
p-HDAC4/ HDAC4
p-ULK1/ ULK1
p-MFF/ MFF
p-Beclin-1/ Beclin-1
p-TBC1D1/ TBC1D1
h
AXIN2+/+
AXIN2-/-
siAXIN1 - - + + - - + +
Glc (mM) 25 0 25 0 25 0 25 0
IB: p-AMPKα
AMPKα
p-ACC
ACC
AXIN1
AXIN2
Tubulin
HEK293T
i
AXIN1+/+
AXIN1-/-
HA-AXIN2 - - + + - - + +
Glc (mM) 25 0 25 0 25 0 25 0
IB: p-AMPKα
AMPKα
p-ACC
ACC
AXIN1
HA (AXIN2)
Tubulin
MEFs

Fig 1

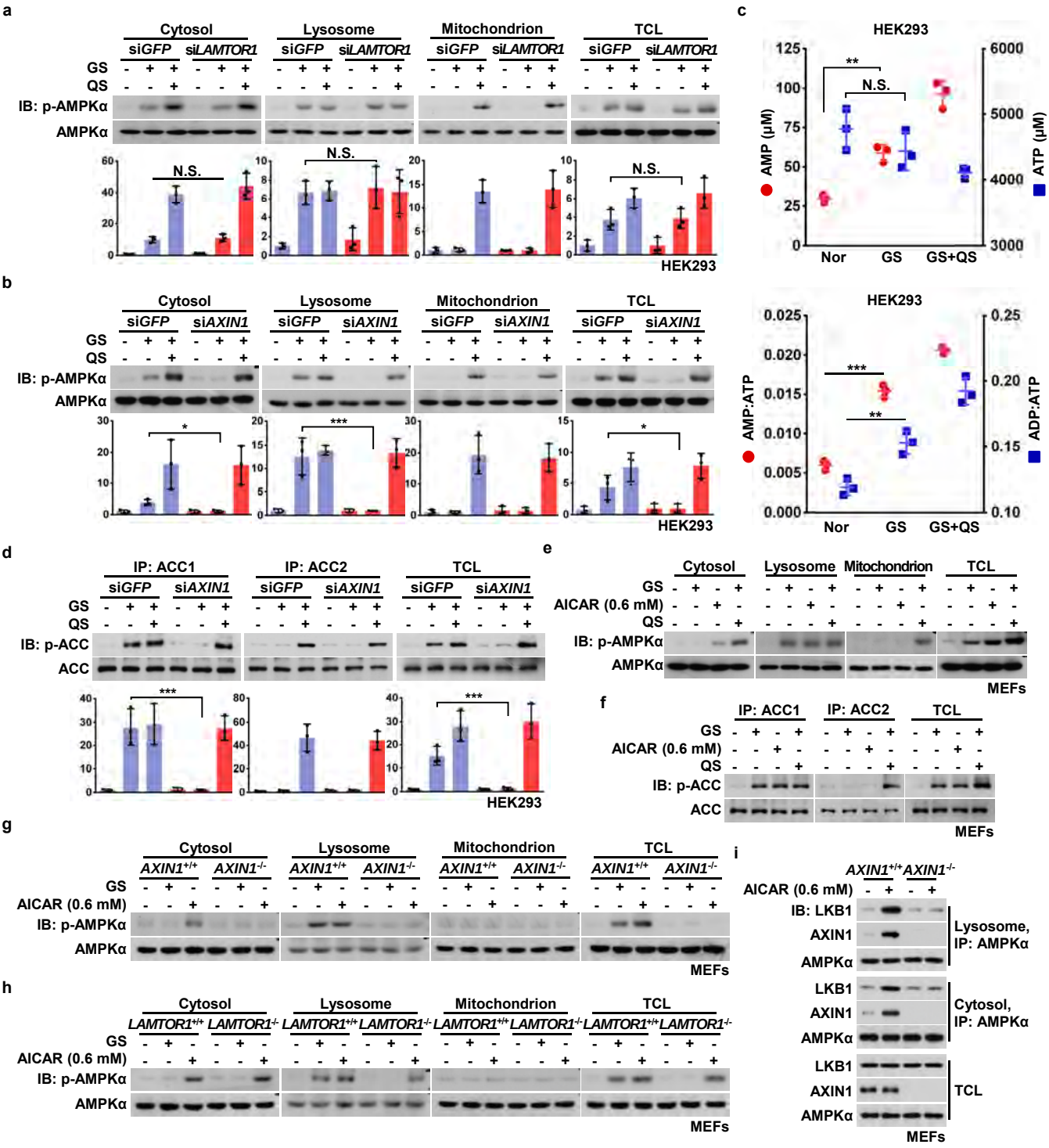
a
Cytosol
Lysosome
Mitochondrion
TCL
siGFP
siLAMTOR1
GS
QS
IB: p-AMPKα
AMPKα
N.S.
HEK293
b
siAXIN1
*
***
c
HEK293
AMP (μM)
ATP (μM)
**
Nor
GS
GS+QS
AMP:ATP
ADP:ATP
d
IP: ACC1
IP: ACC2
IB: p-ACC
ACC
e
AICAR (0.6 mM)
MEFs
f
g
AXIN1+/+
AXIN1-/-
h
LAMTOR1+/+
LAMTOR1-/-
i
IB: LKB1
AXIN1
Lysosome, IP: AMPKα
Cytosol, IP: AMPKα
TCL

Fig 2

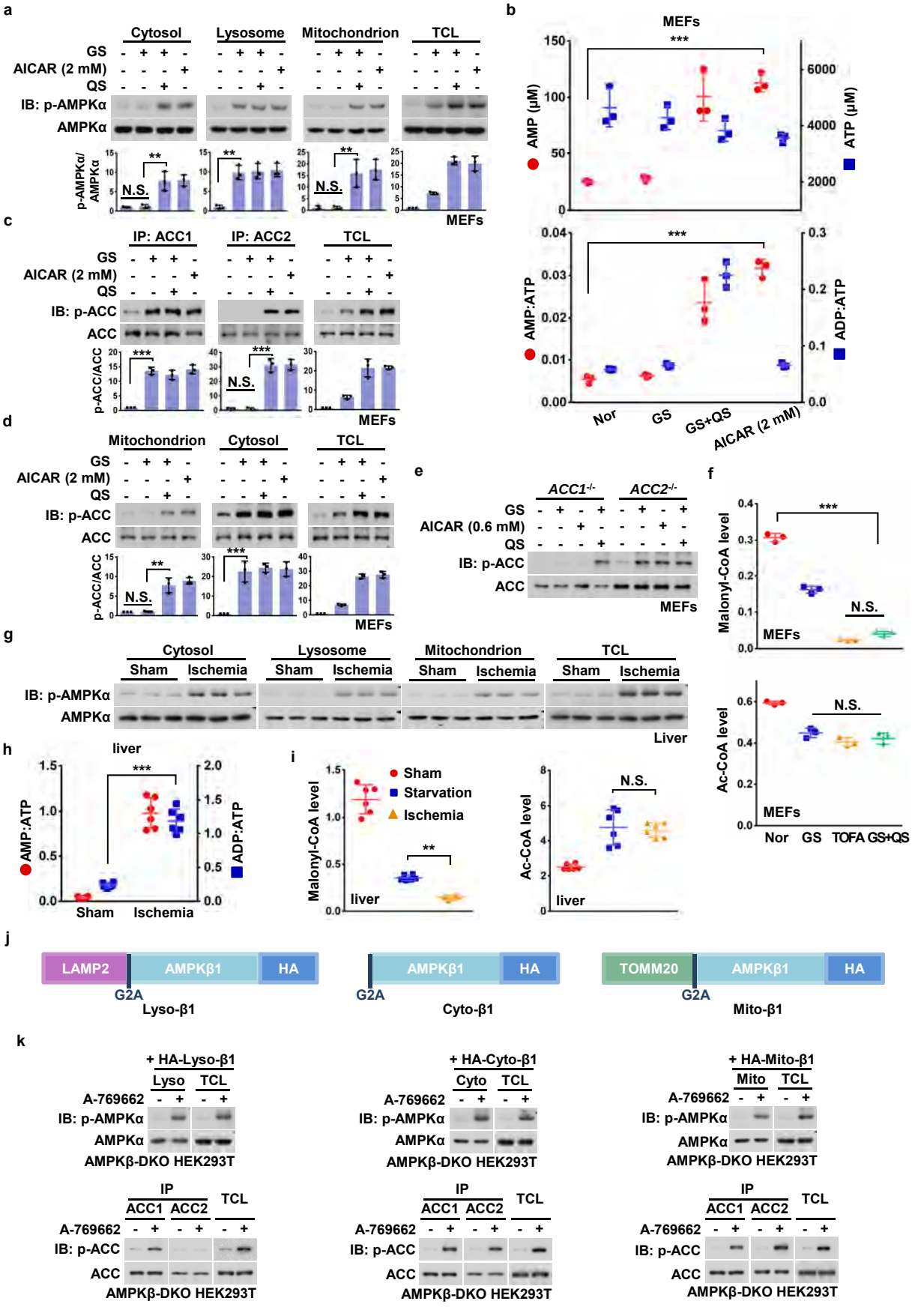
a
Cytosol
Lysosome
Mitochondrion
TCL
GS
AICAR (2 mM)
QS
IB: p-AMPKα
AMPKα
p-AMPKα/ AMPKα
N.S.
MEFs
b
MEFs
AMP (μM)
ATP (μM)
AMP:ATP
ADP:ATP
Nor
GS
GS+QS
AICAR (2 mM)
c
IP: ACC1
IP: ACC2
TCL
IB: p-ACC
ACC
p-ACC/ACC
MEFs
d
Mitochondrion
Cytosol
TCL
MEFs
e
ACC1-/-
ACC2-/-
AICAR (0.6 mM)
MEFs
f
Malonyl-CoA level
Ac-CoA level
MEFs
Nor
GS
TOFA
GS+QS
g
Sham
Ischemia
Liver
h
liver
Sham
Ischemia
i
Sham
Starvation
Ischemia
Malonyl-CoA level
Ac-CoA level
liver
j
LAMP2
AMPKβ1
HA
G2A
Lyso-β1
Cyto-β1
TOMM20
Mito-β1
k
+ HA-Lyso-β1
+ HA-Cyto-β1
+ HA-Mito-β1
Lyso
Cyto
Mito
A-769662
AMPKβ-DKO HEK293T
IP
ACC1
ACC2

Fig 3

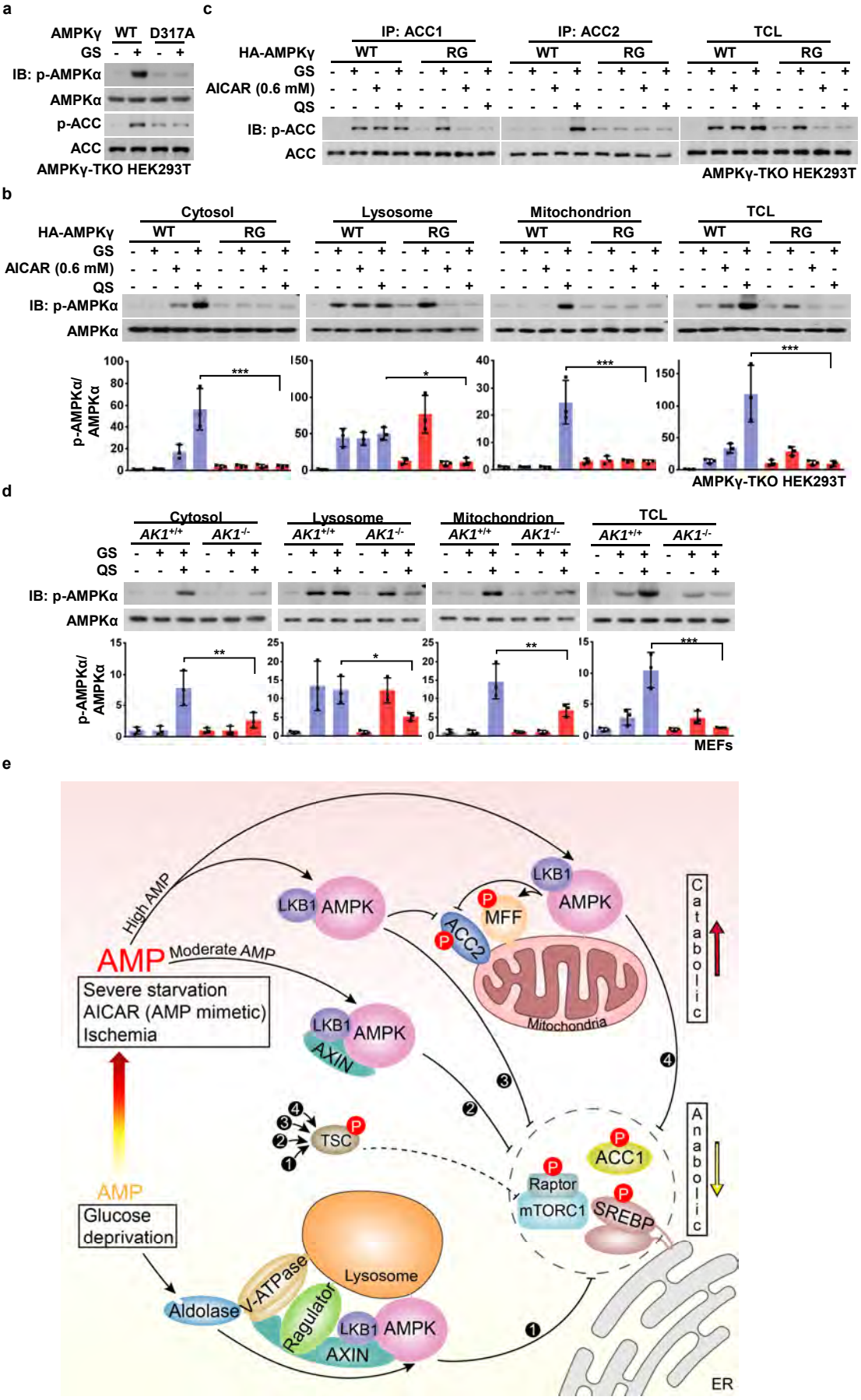
a
AMPKγ WT D317A
GS - + - +
IB: p-AMPKα
AMPKα
p-ACC
ACC
AMPKγ-TKO HEK293T
c
IP: ACC1
IP: ACC2
TCL
HA-AMPKγ WT RG WT RG WT RG
GS
AICAR (0.6 mM)
QS
IB: p-ACC
ACC
AMPKγ-TKO HEK293T
b
Cytosol
Lysosome
Mitochondrion
TCL
HA-AMPKγ WT RG WT RG WT RG WT RG
GS
AICAR (0.6 mM)
QS
IB: p-AMPKα
AMPKα
p-AMPKα/ AMPKα
AMPKγ-TKO HEK293T
d
Cytosol
Lysosome
Mitochondrion
TCL
AK1+/+ AK1-/-
GS
QS
IB: p-AMPKα
AMPKα
p-AMPKα/ AMPKα
MEFs
e
High AMP
AMP
Moderate AMP
Severe starvation
AICAR (AMP mimetic)
Ischemia
LKB1 AMPK
AXIN
MFF
ACC2
Mitochondria
Catabolic
TSC
Raptor
mTORC1
ACC1
SREBP
Anabolic
AMP
Glucose deprivation
Aldolase
V-ATPase
Ragulator
Lysosome
ER

Fig 4

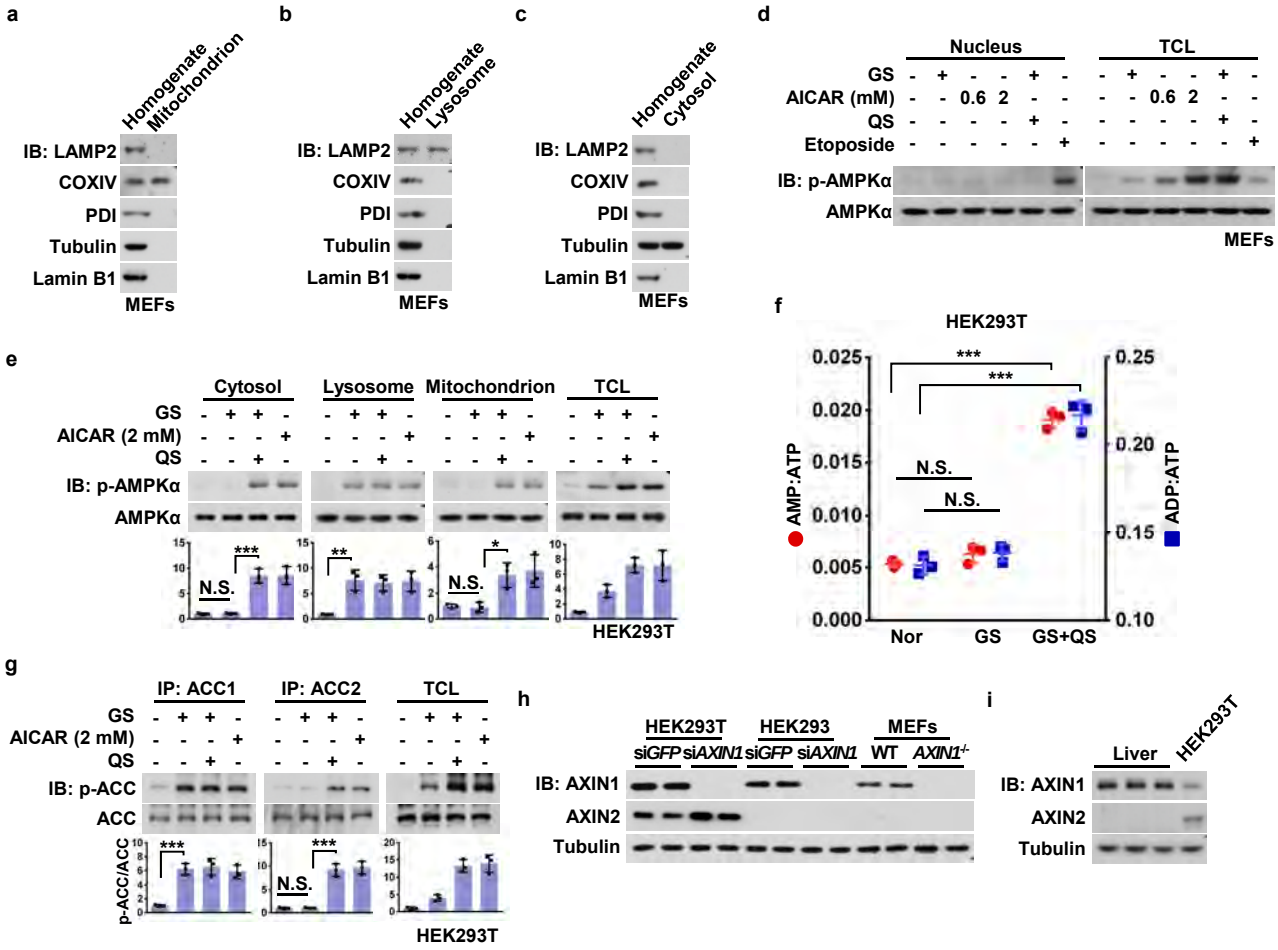

Supplementary information, Fig. S1. Basal AMP Is Sufficient for Activation of the Lysosomal Pool of AMPK

(**a-c**) Validation of methods for subcellular fractionation. MEFs were homogenized and subjected to fractionation of mitochondrion (**a**), lysosome (**b**) and cytosol (**c**) following individual methods (described in "Materials and Methods" section). Fractions were then analyzed by immunoblotting using the antibodies against LAMP2 (a lysosome marker), COXIV (a mitochondrion marker), PDI (an ER marker), tubulin (a cytosol marker) and Lamin B1 (a nuclear marker), respectively.

(**d**) No nuclear AMPK activation can be detected under glucose starvation or severe nutrient stress. MEFs were starved for glucose, glucose and glutamine, treated with 0.6 or 2 mM AICAR, or 20 μM etoposide (all for 2 hr). The nucleus fraction was then prepared, followed by analysis of p-AMPKα levels by immunoblotting.

(**e**) Low glucose exclusively activates lysosomal pool of AMPK in HEK293T cells. Cells were starved for glucose, or for both glucose and glutamine, or treated with 2 mM AICAR, all for 2 hr, followed by fractionation and immunoblotting.

(**f**) Adenine nucleotide ratios are unaltered in HEK293T cells after glucose starvation. Cells were starved as in (**e**), followed by determination of adenylate nucleotide ratios by CE-MS. Results are mean ± SD; *** $p < 0.001$, N.S., not significant by ANOVA, $n = 3$.

(**g**) ACC1, but not ACC2, is phosphorylated in in HEK293T cells starved for glucose. Cells were starved or treated with AICAR as in (**e**). Endogenous ACC1 and ACC2 were individually immunoprecipitated, followed by immunoblotting.

(**h, i**) AXIN2 can be readily detected in HEK293T cells but not in MEFs, HEK293 cells and mouse liver. MEFs, HEK293 cells, HEK293T cells (with AXIN1 knocked down/knocked out as controls) and mouse liver were lyzed and analyzed by immunoblotting.

Experiments in (**a**), (**b**), (**c**), (**d**), (**f**), (**h**), and (**i**) were performed twice and those in (**e**) and (**g**) three times.

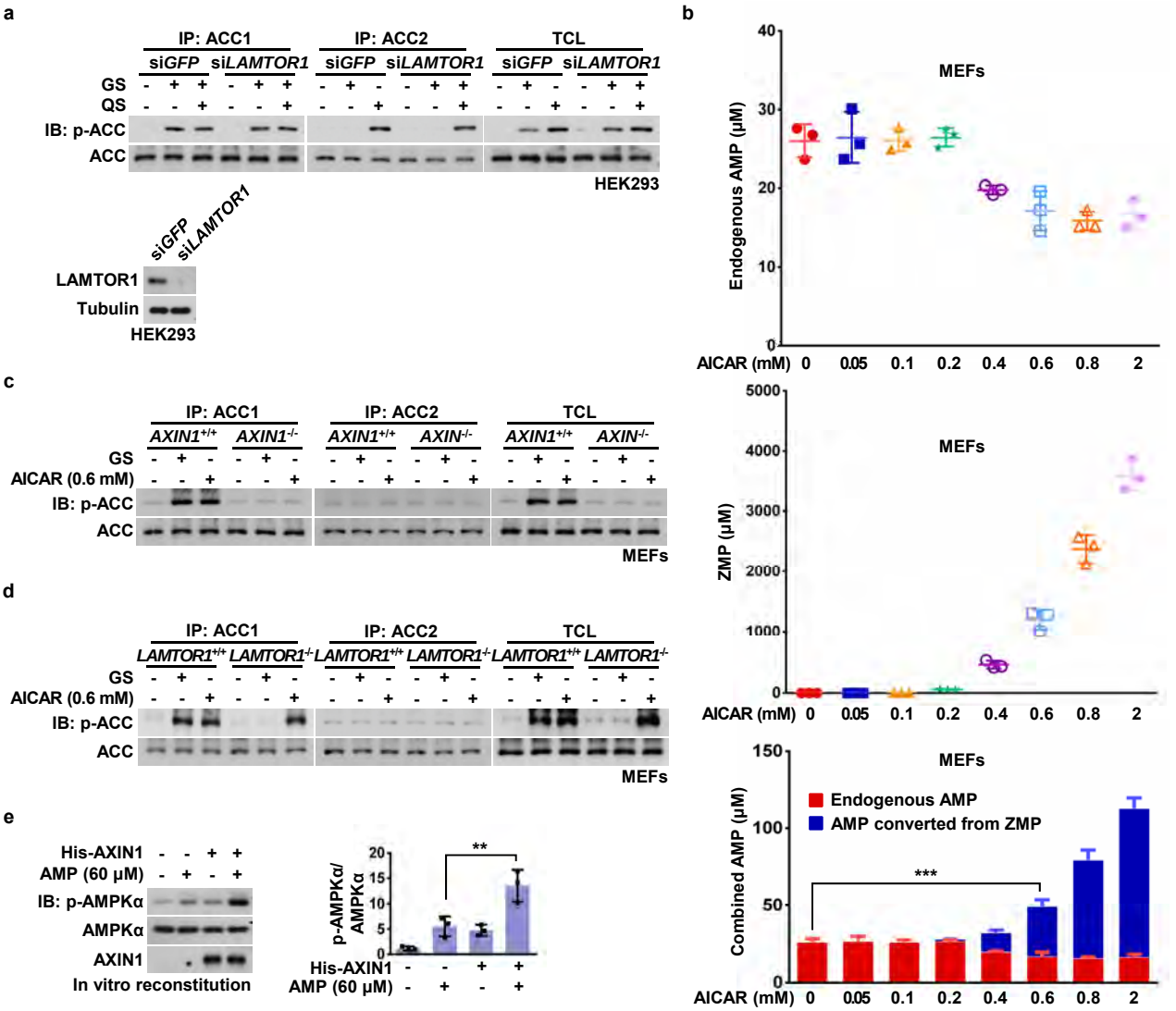

Figure S2

(legend on next page)

Supplementary information, Fig. S2. Modest Increases in AMP Activate Cytosolic AMPK in an AXIN1-dependent Manner

(**a**) ACC1, but not ACC2, is phosphorylated in HEK293 cells after glucose starvation in a LAMTOR1-independent manner. Cells were glucose-starved or severely starved as in Fig. 2a, in which endogenous ACC1 and ACC2 were immunoprecipitated and analyzed by immunoblotting.

(**b**) ZMP and AMP levels in MEFs treated with AICAR. MEFs were treated with AICAR at indicated concentrations for 2 hr, levels of the endogenous AMP (top panel), AICAR-generated ZMP (middle panel) were then determined by CE-MS, and the combined AMP levels are shown in the bottom panel. Results are mean ± SD; *** $p < 0.001$ by ANOVA, n = 3.

(**c-d**) Phosphorylation of ACC1 by low concentrations of AICAR is dependent on AXIN1, but not LAMTOR1. *AXIN1*$^{-/-}$ MEFs (**c**) and *LAMTOR1*$^{-/-}$ MEFs (**d**) were treated with AICAR or severely starved as in Fig. 2e, followed by immunoprecipitation of ACC1 or ACC2, and analyzed by immunoblotting.

(**e**) Moderate levels of AMP significantly promotes the phosphorylation of AMPK by LKB1 in vitro in an AXIN1-dependent manner. Bacterially expressed and purified AMPK (800 ng) was incubated with active LKB1/MO25/STRAD complex (200 ng) at 32 ° C, 15 min in a kinase buffer containing 5 mM ATP with or without 60 μM AMP and 1 μg of AXIN. Phosphorylation of AMPK was determined by immunoblotting.

All experiments were performed twice except for that in (**a**) three times.

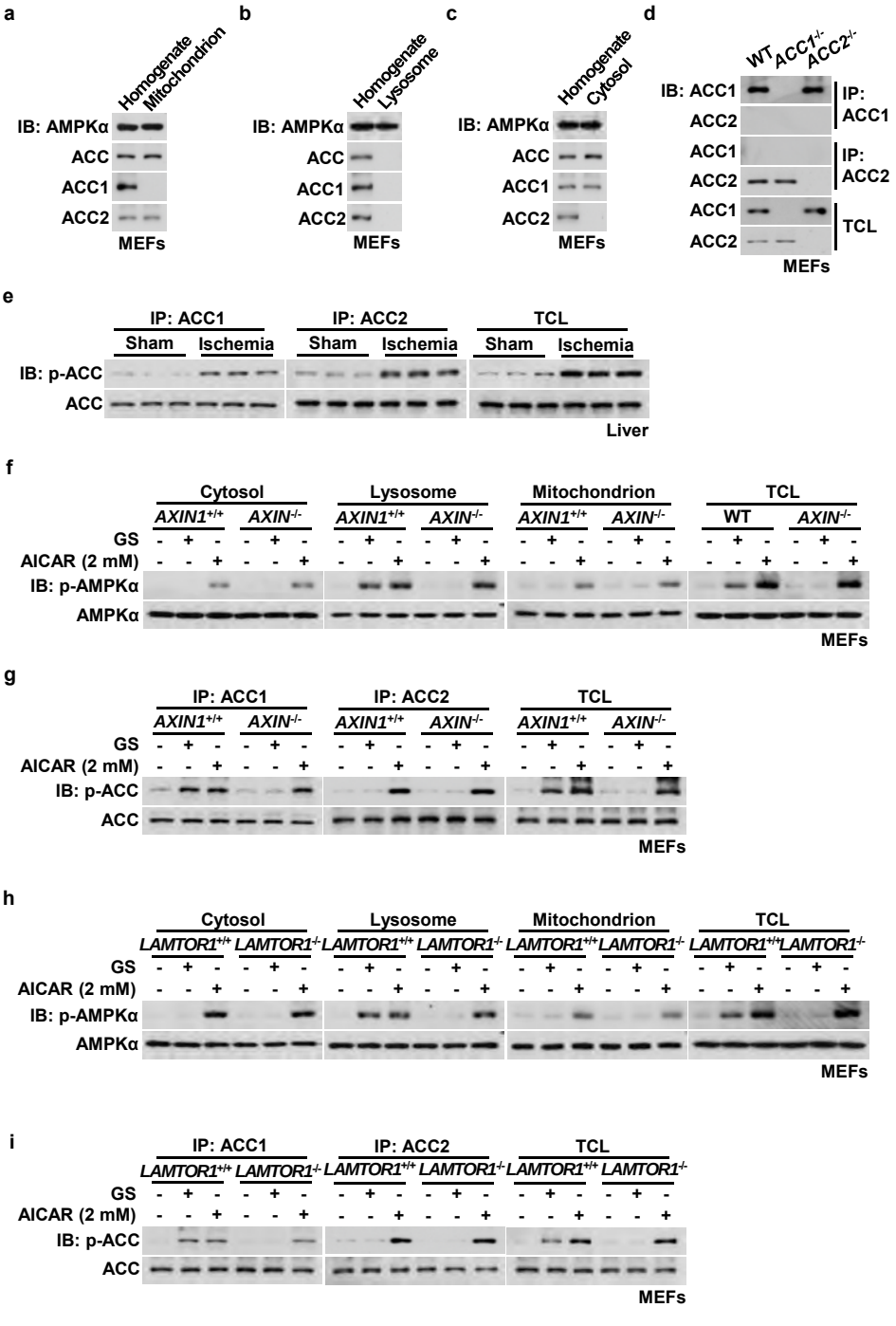

Figure S3

(legend on next page)

Supplementary information, Fig. S3. The Mitochondrion-localized ACC2 Is Phosphorylated by AMPK Only after Severe Nutrient Stress

(**a-c**) ACC2 is a mitochondrion-residential protein. MEFs were homogenized and subjected to fractionation of mitochondrion (**a**), lysosome (**b**) and cytosol (**c**). Fractions were then analyzed by immunoblotting using antibodies indicated. Note that neither ACC1 nor ACC2 could be detected on the lysosomal fraction.

(**d**) Validation of *ACC1*$^{-/-}$ and *ACC2*$^{-/-}$ MEFs, and the specificity of antibodies against ACC1 and ACC2. MEFs with *ACC1* or *ACC2* knocked out, or wildtype MEFs as a control, were lyzed and immunoprecipitated using antibodies against ACC1 and ACC2, respectively. The immunoprecipitates, along with the total lysates, were analyzed by immunoblotting.

(**e**) Both ACC1 and ACC2 can be phosphorylated in the liver of mice after hepatic ischemia. Mice were anesthetized, and the left lateral and median lobes of the liver were deprived of blood flow as in Fig. 3g. Liver samples were then homogenized and immunoprecipitated for ACC1 and ACC2, respectively, followed by immunoblotting.

(**f, g**) Knockout of *AXIN1* does not affect the activation of mitochondrion- and cytosol-localized AMPK, and the phosphorylation of ACC2 in high AMP conditions. MEFs with *AXIN1* knocked out were deprived of glucose or both glucose and glutamine for 2 hr, followed by fractionation and immunoblotting for analyzing p-AMPKα (**f**), or by immunoprecipitation and immunoblotting for analyzing p-ACC1 and p-ACC2 (**g**).

(**h, i**) Knockout of *LAMTOR1* does not affect the activation of mitochondrion- and cytosol-localized AMPK, and the phosphorylation of ACC2 in high AMP conditions. MEFs with *LAMTOR1* knocked out were deprived of glucose or both glucose and glutamine as in (**f**), followed by analyzing p-AMPKα (**h**), or p-ACC1 and p-ACC2 (**i**).

All experiments were performed twice except for that in (**e**) three times.

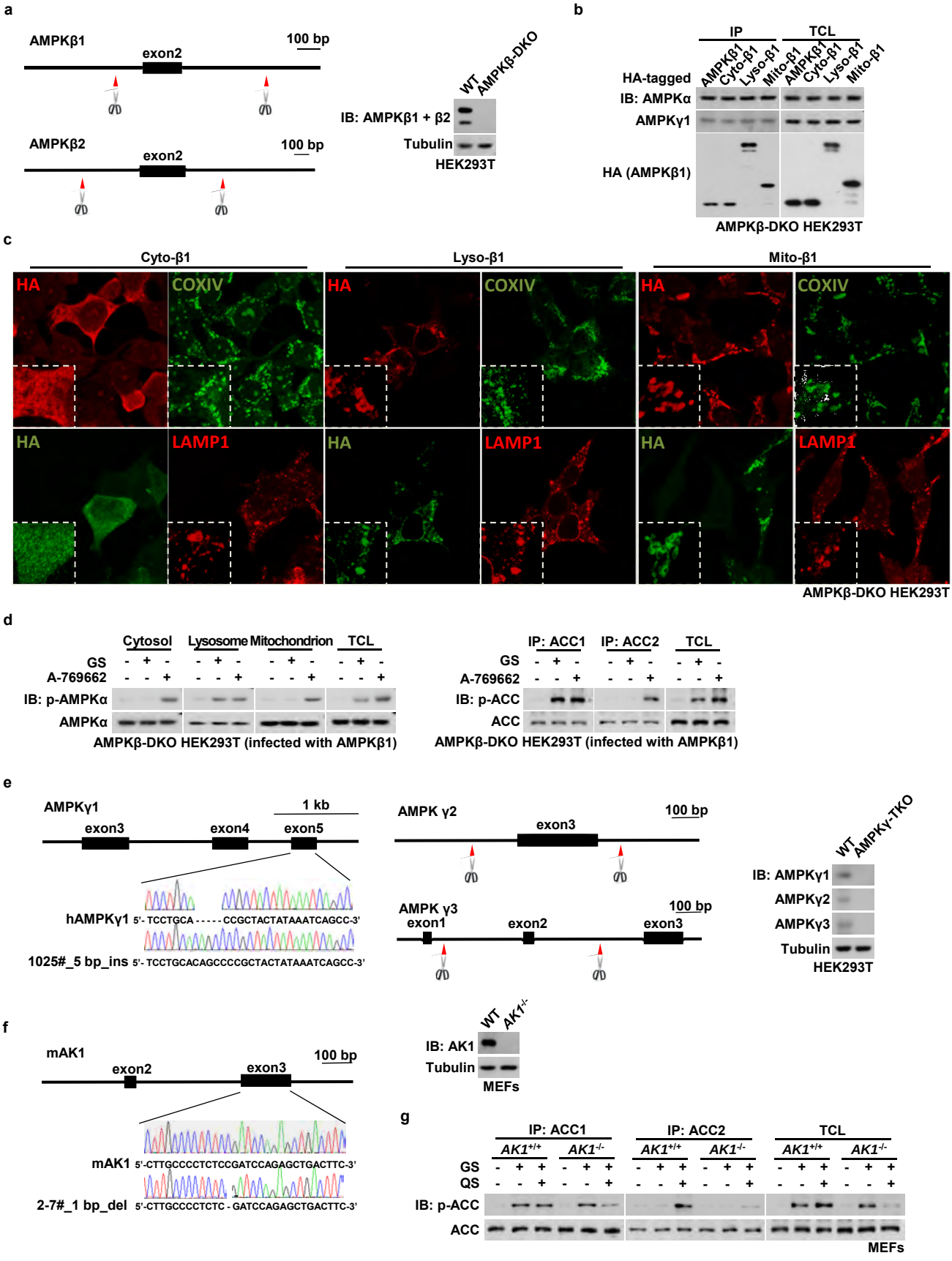

Figure S4

(legend on next page)

Supplementary information, Fig. S4. Roles of AMP in the Hierarchical Activation of AMPK

(**a**) Generation and validation of AMPKβ-DKO HEK293T cells. The strategy to generate AMPKβ-DKO HEK293T cells was shown on left panel. For validation, HEK293T cells with AMPKβ1 and AMPKβ2 knocked out were lyzed, followed by analyzing protein levels of AMPKβ1 and AMPKβ2 by immunoblotting using an antibody against both isoforms (shown on right panel).

(**b**) The expressed proteins of fusion constructs of the β1 subunit are effectively assembled into heterotrimeric AMPK complexes. AMPKβ-DKO HEK293T cells were infected with HA-tagged lyso-β1, cyto-β1 and mito-β1, respectively. Cells were lyzed, followed by immunoprecipitation with antibody against HA tag, and then subjected to immunoblotting using antibodies indicated.

(**c**) Validation of the subcellular localization of the β1-fusion constructs. AMPKβ-DKO HEK293T cells were infected with the lyso-β1 and mito-β1 fusion constructs, followed by immunofluorescent staining using antibodies indicated.

(**d**) A-769662 successfully causes activation of AMPK in AMPKβ-DKO HEK293T cells re-introduced with AMPKβ1. Cells were treated with 1 μM A-769662 for 2 hr, and then by fractionation and immunoblotting for analyzing p-AMPKα (left panel), or by immunoprecipitation and immunoblotting for analyzing p-ACC1 and p-ACC2 (right panel).

(**e, f**) Generation and validation of AMPKγ-TKO HEK293T cells and *AK1*$^{-/-}$ MEFs. Strategies to generate the two lines of cells were shown on left of each panel, with validation of each cell line by immunoblotting using antibodies indicated (shown on right of each panel).

(**g**) Knockout of *AK1* significantly dampens the phosphorylation of ACC2 in high AMP conditions. MEFs with *AK1* being knocked out were deprived of glucose or both glucose and glutamine for 2 hr, followed by immunoprecipitation and immunoblotting for analyzing p-ACC1 and p-ACC2.

Experiments in (**d**) were performed three times and others twice.